ISSN 0140-3818
SSSU 72

UNIVERSITY OF SOUTHAMPTON

DEPARTMENT OF SHIP SCIENCE

FACULTY OF ENGINEERING AND APPLIED SCIENCE

THEORETICAL PREDICTION OF THE WAVE RESISTANCE OF SLENDER HULL FORMS IN CATAMARAN CONFIGURATIONS

A.F. Molland, J.F. Wellicome and P.R. Couser

Ship Science Report 72

March 1994

Theoretical Prediction of the Wave Resistance of Slender Hull Forms in Catamaran Configurations

A.F. Molland, J.F. Wellicome and P.R.Couser

Ship Science Report No. 72
University of Southampton

March 1994

Contents

Nomenclature

Symbols and some values used in the report:

Demihull	One of the hulls which make up the catamaran
Fn	Froude Number, $[v/\sqrt{gL}]$
Rn	Reynolds Number, $[vL/\nu]$
v, U, $\boldsymbol{U}$	Velocity [ms^{-1}]
W	Tank width
H	Tank depth
L, L_{BP}	Demihull length between perpendiculars [m]
A	Static wetted surface area [m^2]
B	Demihull maximum beam [m]
T	Demihull draught [m]
T_{trans}	Draught at transom [m]
b	Local beam
z	Local depth
S	Separation between catamaran demihull centrelines [m]
∇	Volume of displacement [m^3]; Differential operator
Δ	Mass displacement in freshwater [kg]
C_B	Block coefficient
C_P	Prismatic coefficient
$L/\nabla^{\frac{1}{3}}$	Length : displacement ratio, $[L/\nabla^{\frac{1}{3}}]$
R_T	Total resistance
C_T	Coefficient of total resistance $[R_T/\ \frac{1}{2}\ \rho A v^2]$
R_W	Wave resistance
C_W	Coefficient of wave resistance $[R_W/\ \frac{1}{2}\ \rho A v^2]$
R_{WP}	Wave pattern resistance
C_{WP}	Coefficient of wave pattern resistance $[R_{WP}/\ \frac{1}{2}\ \rho A v^2]$
C_F	Coefficient of frictional resistance [ITTC-57 Correlation line]
R_{trans}	Transom resistance
R	A measurement of resistance
$1+k$	Form factor
β	Viscous resistance interference factor
τ	Wave resistance interference factor
t	time
$f(x,z)$	hull shape
Φ	Total velocity potential
ϕ	Velocity potential
ζ	Free surface elevation
$K_0 = g/U^2$	Fundamental Wave number (deep water)
m	Harmonic number
K_m	Wave number
θ_m	Wave angle
σ	Source strength
$\hat{\boldsymbol{n}}$	unit normal vector
r	Distance to source
g	Acceleration due to gravity [9.80665 ms^{-2}]
ρ	Density of freshwater [1000 kg/ m^3]
ν	Kinematic viscosity of freshwater [1.141×10^{-6} m^2s^{-1} at 15°C]

1 Introduction

The commercial applications of high speed displacement catamarans has increased significantly over the past few years. Little information is, however, available for carrying out powering estimates for such vessels, particularly in the high speed range.

Work on the resistance of high speed displacement catamarans has been ongoing over a number of years at the University of Southampton[3, 4] in an effort to improve the understanding of their resistance components and to provide design data.

This report describes the development of theoretical methods for the prediction of the wave resistance of catamarans.

The basic objectives of the theoretical investigation were to develop and improve the prediction capabilities of an existing slender body wave resistance theory for catamaran hulls, reported in[3, 4]. In particular, it was necessary to improve the prediction of wave resistance amplitude and the phasing of the humps and hollows in the resistance curve, and to validate the theory over a wider range of hull parameters. As such, it would then offer wider applications as a design tool.

In attempting to improve the prediction capabilities a number of investigations were carried out which entailed improving the method of mathematically defining the hull, investigating the sensitivity of wave resistance to changes in the number and distribution of source panels, incorporating suitable allowances for running trim and sinkage effects and improving the modelling of the transom effects. A background to the theory and description and discussion of the investigations carried out are given in the following sections.

The work described formed part of a wider research programme, funded by SERC through MTD Ltd. over a two year period, which included an extensive series of model resistance tests on catamarans in calm water. The experimental work is the subject of a separate report[6].

2 Background to Theory

The theory is based on linearised analysis of the far field wave pattern generated by an arbitrary array of Kelvin sources in a finite channel. Thin ship assumptions are used to relate source strength to hull form shape. See Equation 1.

$$\sigma = \frac{-1}{2\pi} \hat{\boldsymbol{n}} \cdot \boldsymbol{U} \times \text{panel area} \tag{1}$$

where $\hat{\boldsymbol{n}}$ is the outward unit normal vector of the panel and $\boldsymbol{U}$ is the onset free stream.

Eggers wave coefficients are obtained and the resistance obtained from these coefficients. The method can be applied to any slender hull shape and any number of hulls in the tank. Modifications to the basic theory are required to take account of transom sterns, sinkage and trim. A full description of the development of the theory in given by Insel[3] and a detailed summary is given in Appendix A. An outline of the numerical implementation is given in Appendix B

3 Modifications to Existing Theory

Areas of the numerical model where improvements were thought necessary included:

- Hull definition
- Panel density and distribution
- Running trim and sinkage
- Modifications caused by transom stern

These modifications are described in the following sections.

3.1 Mathematical hull definition

The theoretical investigation was based on the same NPL round bilge transom stern models used in the experimental investigation. The basic hull forms were defined by parametric cubic spline curves which could be interpolated to provide coordinate data at any point on the hull. This facilitated the definition of the coordinates of the source panels, both when investigating the number of panels used and when redefining the distribution of panels due to sinkage and trim.

3.2 Number, distribution and definition of basic source panels

For the numerical representation of the hull it was necessary to discretise the hull into panels governed by the choice of the numbers of waterlines and sections. Systematic studies were carried out to investigate the effects of changes in numbers and distribution of the source panels.

It was found that above about 18 waterlines and 30 sections the differences in predicted results became very small as the number of panels was increased. The use of non-parallel (fanned) waterlines was also investigated as this approach provides better geometric coverage of typical transom stern / round bilge craft profiles. Compared with using parallel waterlines this approach was found to lead to some changes in predicted resistance. However, when running trim was taken into account the effect of fanning the waterlines was negligible since the waterline and keel profile were virtually parallel and the investigation was discontinued. The distribution finally adopted for the calculations was horizontal waterlines and vertical sections with 20 depthwise panels and 50 lengthwise panels.

An investigation was also carried out to compare the representation of each panel by either a point source or a constant source distribution over the panel. It was found that providing the hull was subdivided with a fine enough mesh, say of order 20×50 mentioned above, both methods gave very similar results. It could also be argued that point sources were sufficient since the far field only was of interest. For speed of calculation the point source method was therefore retained.

3.3 Effects of running trim and sinkage

Running trim and sinkage can be calculated by integration of the pressures over the hull panels, but this approach is computationally expensive when applied to thin ship theory since the method then requires evaluation of the near field velocity and pressure terms.

Extensive experimental values for the running trim and sinkage had been acquired in the course of the research[6]. Since one of the required outcomes of the theoretical model was its use as a practical design tool, it was considered that the more realistic approach would be to incorporate the experimental values of trim and sinkage in the theoretical model. The approach adopted has been to redefine the hull into the running hull shape by taking the running trim and sinkage into account and then to generate source panels for the modified hull form. A planar water line was used and the wave profile along the hull was not simulated.

3.4 Modelling transom stern effects

A transom stern correction is necessary because source panels were not applied over the transom in the slender body approximation leaving the model 'open'. This caused the numerical scheme to under predict the wave resistance. The model was 'closed' in several ways, discussed below, in order to make up this deficit.

A transom stern correction modelled using a hydrostatic term had been adopted in the existing program with reasonable success (see Equation 2). It was however considered that this approach could be improved upon, and that alternative corrections should be investigated. In particular, the effects of sinks or sink line distributions in various proximities to the transom would be explored.

$$R_{\text{trans}} = \rho g \int_0^{T_{\text{trans}}} z.b(z)\, dz \tag{2}$$

where T_{trans} is the transom draught and $b(z)$ defines the beam of the transom at depth z.

Various approaches were investigated including a transverse sink line along the bottom of the transom, similar to that used by Yim[9] (where the source strength was given by Equation 3), a single sink at various positions on the centreline of the transom or in its proximity and a single line or array of sinks extending aft into the wake. For the latter cases the source strength was determined by the requirement to achieve zero net source strength around the hull (ie: $\sum \sigma_{\text{body}} + \sum \sigma_{\text{transom}} = 0$). Examples of some of the sink arrangements tested are shown in Figure 1. This systematic investigation into alternative superimposed sink distributions was chosen as a satisfactory alternative to attempting the identification of source / sink arrays to match measured wave patterns.

$$\delta\sigma\,(L, \pm b, z(b)) = \frac{-U}{4\pi}\, z(b)\, \delta b \tag{3}$$

where two sources of strength $\delta\sigma$ were placed at the longitudinal position of the transom ($x = L$), either side of the centre plane ($y = \pm b$), and at a depth corresponding to the transom depth $z(b)$ at $y = b$.

The outcome of the investigation was disappointing since, although the results for the single transom sink and transom sink lines were promising, leading to phase shifts and corrective modifications to the resistance curves, improvements over the hydrostatic correction were not significant. Since all the methods were basically modelling the transom running clear it was apparent that none would adequately model the lower speed range, and that reasonable results in this range could only be achieved by empirical corrections.

A further, slightly different, approach for 'closing' the transom was also investigated. This occurred late in the contract and only a preliminary investigation was possible. The method involved the addition of a virtual appendage to the transom which enclosed the separated flow in the low speed range and the air pocket in the high speed range. Initial investigations were promising and gave good approximations to the wave pattern resistance. For practical powering prediction wave pattern resistance is perhaps not

as useful as wave resistance ($C_T - (1+k)C_F$), although it is likely to give a better description of the actual physical flow. A more detailed description of this method and initial results are given in Appendix C.

Results of theoretical predictions using the various methods are given in Figure 2.

4 Comparison of the Numerical Results with Experimental Data

Comparisons were made with the experimental data[6], including the effects of Length:Displacement Breadth:Draught (B/T) and Separation:Length (S/L) ratios. Overall, reasonable results were obtained and the trends correctly predicted for Froude Number greater than about 0.4. Below Froude Number of 0.4 (before the transom started to run clear) the predictions differ from the experimental results quite significantly in places. Examples of comparisons between theory (using the transverse sink line transom correction) and experiment are given in Figures 3 to 5.

Figures 3a, b, c, and d shows comparisons between experimental and predicted total resistance coefficient (C_T) for the four Length:Displacement ratios investigated. Comparisons are made for the monohull in all cases. It can be seen that for the highest displacement model (3b) there are some discrepancies between observed and predicted values. However these errors rapidly diminish as the Length:Displacement ratio increases, and very good correlation is found for Models 5b and 6b. This is as expected since these more slender hulls better fit the numerical assumptions and approximations implied in the slender body model. As mentioned above the predicted results for Froude Number less than 0.4 are poor since this is the region in which the transom is *not* running clear.

Figures 4a, b and c show how the method predicts changes in B/T. Good agreement can be seen in all cases for the higher Froude Number range. Again the results for the monohulls are shown.

Figures 5a, b, c and d show the predictions for four catamarans (Models 5b S/L=0.2, 0.3, 0.4 and 0.5 respectively). Again good agreement is shown for the higher Froude Number Range.

5 Parametric Studies

Figures 6 to 8 show how the predicted wave resistance coefficient (C_W) varies with changes in the design parameters, and represent examples of parametric studies which might typically be used for design purposes. Figure 6a shows the prediction of the way in which hull separation affects the C_W.This can be compared with the experimental results in Figure 6b. Figures 7a and 7b show the effect of Length:Displacement ratio and Figures 8a and 8b the effect of B/T. Although the quantitative values of predicted resistance are not fully correct, the numerical procedure can be used in a qualitative manner to investigate the effects of many changes in hull parameters quickly and efficiently at the preliminary design stage.

6 Conclusions

Some improvements in the prediction capabilities of the theory have been achieved. The modifications to include running trim and sinkage have been beneficial to the analysis whilst only small improvements were achieved with the transom correction.

Overall, the method offers the ability to make very reasonable estimates of catamaran wave resistance, particularly in the higher speed range, and provides a very useful practical design tool for parametric studies.

Further attempts at improving the prediction quality of the current approach are likely to be curtailed by the overriding constraints of linearised slender body theory.

Acknowledgements

The work described in this report covers part of a research project funded by SERC through MTD Ltd. under research grant Ref. Nos. GR/H17992, SHP107/MHV 2.

The authors would like to acknowledge the contributions to the work on source panelling and transom corrections made by Dr. M.Insel (during his recent tenure of a Visiting Fellowship in the Department of Ship Science) and Mr. A.Lee (part-time postgraduate in the Department of Ship Science).

References

[1] D. Bailey. The NPL high speed round bilge displacement hull series. Maritime Technology Monograph 4, Royal Institution of Naval Architects, 1976.

[2] G.K. Batchelor. A proposal concerning wakes behind bluff bodies at large reynolds numbers. *Journal of Fluid.Mechanics*, 6:547–567, November 1959.

[3] M. Insel. *An Investigation into the Resistance Components of High Speed Displacement Catamarans.* PhD thesis, University of Southampton, 1990.

[4] M. Insel and A.F. Molland. An investigation into the resistance components of high speed displacement catamarans. *Transactions of the Royal Institution of Naval Architects*, 1992.

[5] J.H. Mitchell. The wave resistance of a ship. *Philosophical Magazine, London, Series 5*, 45(272):106–123, January 1898.

[6] A.F. Molland, J.F. Wellicome, and P.R. Couser. Resistance experiments on a systematic series of high speed displacement catamaran forms: Variation of length-displacement ratio and breadth-draught ratio. Ship Science Report No. 71, Department of Ship Science, University of Southampton, March 1994.

[7] S.N. Sinha. Backward facing step flow experiments. *AIAA Journal*, 19:1527–1530, 1981.

[8] J.V. Wehausen. The wave resistance of ships. *Advances in Applied Mechanics*, 1973.

[9] Bohyun Yim. Analyses of waves and the wave resistance due to transom-stern ships. *Journal of Ship Research*, June 1969.

- Hull surface, no penetration condition

$$\frac{df}{dt} = (U + \phi_x)f_x + \phi_y f_y + \phi_z f_z = 0$$

or, in linearised form:

$$U f_x + \phi_y = 0 \text{ , on } y = f(x,z) \tag{10}$$

- Radiation condition; waves do not propagate upstream of the model:

$$\lim_{(x^2+y^2)\to\infty} \phi = \mathrm{O}(1) \text{ , for } x > 0$$

$$\lim_{(x^2+y^2)\to\infty} \phi = 0 \text{ , for } x < 0 \tag{11}$$

A.2 Velocity Potential of a Source in a Finite Channel

By working from the velocity potential of a source in shallow, unbounded water of depth H, given by Wehausen[8], Insel[3] shows that the velocity potential of a source of strength σ, located at (x_0, y_0, z_0), in a finite channel is given by:

$$\phi = -\sigma J_1 + \frac{4\sigma}{\pi} J_2 + 4\sigma J_3 \tag{12}$$

where the terms that appear in equation 12 are given below.

$$J_1 = \sum_{n=-\infty}^{\infty} \left[\frac{1}{r_1'} + \frac{1}{r_1''} + \frac{1}{r_2'} + \frac{1}{r_2''} \right] \tag{13}$$

$$r_1' = \sqrt{(x-x_0)^2 + (y-y_0')^2 + (z-z_0)^2}$$

$$r_1'' = \sqrt{(x-x_0)^2 + (y-y_0'')^2 + (z-z_0)^2}$$

$$r_2' = \sqrt{(x-x_0)^2 + (y-y_0')^2 + (z+2H+z_0)^2}$$

$$r_2'' = \sqrt{(x-x_0)^2 + (y-y_0'')^2 + (z+2H+z_0)^2}$$

Note: image sources are located at (x_0, y_0', z_0) and (x_0, y_0'', z_0), where

$$y_0' = y_0 + 2nW \text{ , for } n = -\infty \ldots \infty$$

$$y_0'' = -y_0 + (2n+1)W \text{ , for } n = -\infty \ldots \infty$$

$$J_2 = \frac{2\pi}{W} \int_0^\infty \sum_{m=0}^{\infty}{}' \frac{e^{-kH}\cosh(k(H+z_0))(k + K_0 \sec^2\theta_m)}{\cosh(kH)(k - K_0 \tanh(kH)\sec^2\theta_m)} cosh(k(z+H)) \frac{\cos(k(x-x_0)\cos\theta_m)}{k\cos\theta_m} \left\{ \begin{array}{l} \cos(ky\sin\theta_m)\cos(ky_0\sin\theta_m) \\ \sin(ky\sin\theta_m)\sin(ky_0\sin\theta_m) \end{array} \right\} dk \tag{14}$$

The integral here is the Cauchy principal value integral, with k as the integration variable.

$$J_3 = \frac{2\pi}{W} \sum_{m=0}^{\infty}{}' \frac{e^{-K_m H}\cosh(K_m(H+z_0))(K_0 + K_m\cos^2\theta_m)}{\cosh(K_m H)(1 - K_0 \mathrm{sech}^2(K_m H)\sin^2\theta_m)} cosh(K_m(z+H)) \frac{\sin(K_m(x-x_0)\cos\theta_m)}{K_m\cos\theta_m} \left\{ \begin{array}{l} \cos(K_m y\sin\theta_m)\cos(K_m y_0\sin\theta_m) \\ \sin(K_m y\sin\theta_m)\sin(K_m y_0\sin\theta_m) \end{array} \right. \tag{15}$$

where $\sum'$ denotes that the $m = 0$ term is halved; and the cosine terms apply to even m and the sine terms apply to odd m. and the wave number K_m and wave angle θ_m are found by solving:

$$K - K_0 \sec^2\theta \tanh(KH) = 0$$

and

$$K_m \sin\theta_m = \frac{m\pi}{W}$$

APPENDIX A

A Theoretical Wave Resistance of a Ship Form in a Shallow Water Channel

The linearised wave resistance theory of Mitchell[5] has been used to give comparative results for many years. Here the modified theory used by Insel[3] is described.

The wave field and resistance of a source in a finite channel, given by Insel[3], and its application to the calculation of single and multiple-body wave resistance is described.

A.1 Assumptions and Boundary Conditions

For the linearised potential theory used, the following assumptions are:

- The fluid is inviscid, incompressible and homogeneous.
- The flow is steady and irrotational.
- Surface tension can be neglected
- The free surface elevation is small compared with wave length, and with no wave breaking present.
- All the energy causing free surface waves can be measured by examining the far field wave system.

A cartesian coordinate system, moving with the model, with origin in the undisturbed free surface and model centre line is used. A right-handed system is used with the x-axis in the direction of ship motion; the y-axis to starboard; and the z-axis vertically upwards.

The velocity potential can be described as a summation of the free stream and flow disturbance potentials caused by the body (equation 4).

$$\Phi = Ux + \phi(x, y, z) \tag{4}$$

If the free surface elevation is expressed as $z = \zeta(x, y)$, the under water body geometry as $y = f(x, y)$, and the channel is of depth H and width W; then the following boundary conditions must be satisfied:

- Continuity equation for potential flow:

$$\nabla^2\phi = 0 \tag{5}$$

- Free Surface Conditions:
  - Dynamic free surface condition:

$$g\zeta + U\phi_x + \tfrac{1}{2}(\phi_x^2 + \phi_y^2 + \phi_z^2) = 0$$

    or, in linearised form:

$$g\zeta + U\phi_x = 0 \text{ , on } z = 0 \tag{6}$$

  - Kinematic free surface condition:

$$\frac{d\zeta}{dt} = (U + \phi_x)\zeta_x + \phi_y\zeta_y + \phi_z = 0$$

    or, in linearised form:

$$U\zeta_x - \phi_z = 0 \text{ , on } z = 0 \tag{7}$$

  finally, by combining the two conditions (equations 6 and 7), the linearised free surface condition can be written as:

$$\phi_{xx} + K_0\phi_z = 0 \text{ , on } z = 0 \tag{8}$$

  where $K_0 = \frac{g}{U^2}$

- Bottom, no penetration condition

$$\frac{\partial z}{\partial t} = \phi_z = 0 \text{ , on } z = -H \tag{9}$$

A.3 Far Field Wave System of a Body in a Finite Channel

The far field velocity potential of a source at (x_0, y_0, z_0) can be found by considering the limit as $x \to \infty$ in equation 12.

$$\phi_{\text{ff}} = \lim_{x\to\infty} \phi(x, y, z)$$

$$\phi = -\sigma \lim_{x\to\infty} J_1 + \frac{4\sigma}{\pi} \lim_{x\to\infty} J_2 + 4\sigma \lim_{x\to\infty} J_3 \tag{16}$$

Insel[3] shows that by applying the limit $x \to \infty$ to the terms J_1, J_2 and J_3 (from equations 13, 14, 15) and substituting into equation 16 that the far field velocity profile becomes:

$$\begin{aligned}\phi_{\text{ff}} \;=\; & \frac{16\pi\sigma}{W} {\sum_{m=0}}' \frac{e^{-K_m H}\cosh(K_m(H+z_0))(K_0 + K_m\cos^2\theta_m)}{K_m\cos\theta_m(1 - K_0 H\,\text{sech}^2(K_m H)\sin^2\theta_m)} \\ & \frac{cosh(k(z+H))}{cosh(kH)} \sin(K_m(x-x_0)\cos\theta_m) \begin{cases} \cos(K_m y\sin\theta_m)\cos(K_m y_0\sin\theta_m) \\ \sin(K_m y\sin\theta_m)\sin(K_m y_0\sin\theta_m) \end{cases}\end{aligned} \tag{17}$$

where, again, $\sum'$ denotes that the $m = 0$ term is halved; and the cosine terms apply to even m and the sine terms apply to odd m.

Further, it is shown, that by satisfying the various boundary conditions that the wave amplitude ζ_m for a given harmonic m can be expressed as:

$$\zeta_m^2 = \xi_m^2 + \eta_m^2 \tag{18}$$

where:

$$\begin{aligned}\begin{vmatrix} \xi_m \\ \eta_m \end{vmatrix} \;=\; & \frac{16\pi U}{Wg} \frac{K_0 + K_m\cos^2\theta_m}{1 + \sin^2\theta_m - K_0 H\,\text{sech}^2(K_m H)} \\ & \sum_\sigma \left[\sigma_\sigma e^{-K_m H}\cosh[K_m(H+z_0)]\right] \begin{vmatrix} \cos(K_m x_\sigma\cos\theta_m) \\ \sin(K_m x_\sigma\cos\theta_m) \end{vmatrix} \begin{Bmatrix} \cos\frac{m\pi y_\sigma}{B} \\ \sin\frac{m\pi y_\sigma}{B} \end{Bmatrix}\end{aligned} \tag{19}$$

where the final cosine term applies for even m and the final sine term applies for odd m; the $m = 0$ term is halved. The summation over σ includes all the sources from all the bodies; their positions being at $(x_\sigma, y_\sigma, z_\sigma)$.

The wave resistance of the bodies can be found by substituting the wave amplitude from equation 18 into equation 20 below:

$$R_W = \frac{\rho g W}{4}\left\{\zeta_0^2\left[1 - \frac{2K_0H}{\sinh(2K_0H)}\right] + \sum_{m=1}^{\infty}\zeta_m^2\left[1 - \frac{\cos^2\theta_m}{2}\left(1 + \frac{2K_mH}{\sinh(2K_mH)}\right)\right]\right\} \tag{20}$$

APPENDIX B

B Numerical Implementation

The basic procedure for the numerical implementation of the theory is given below:

```
Input Data
For each run:
    Calculate centres for trim and sinkage of model
    Translate and rotate hull geometries
    Panel hulls
    Calculate source strengths for each panel on each hull
    Calculate transom correction for each hull if applicable
    Estimate viscous drag on each hull
    Output geometry and source strengths
    Calculate constant coefficients and run parameters
    For each harmonic:
        Calculate wave number and angle using Newton Raphson
        Calculate harmonic term
        For each hull:
            For each panel:
                Calculate x,y,z terms
                Update total for wave amplitude
            Next panel
        Next hull
        Calculate resistance for harmonic
        Update total resistance
    Next harmonic
Next run
Output results
```

The wave number K_m and wave angle θ_m are calculated by satisfying two boundary conditions:

Wall reflection condition

$$K_m \sin\theta_m = \frac{m\pi}{W}$$

Wave speed relation

$$K_m \cos^2\theta_m = K_0 \tanh(K_m H)$$

these two conditions can be combined to give:

$$K_m^2 - K_m K_0 \tanh(K_m H) - \frac{m\pi}{W} \tag{21}$$

equation 21 can be solved using Newton Raphson with:

$$f = K_m^2 - K_m K_0 \tanh(K_m H) - \frac{m\pi}{W}$$

$$f' = 2K_m - K_m H K_0 \mathrm{sech}^2(K_m H) - K_0 \tanh(K_m H)$$

and

$$\sin\theta_m = \frac{m\pi}{W K_m}$$

An initial guess can be made assuming deep water, where $\tanh(K_m H) \to 1$ as $H \to \infty$. The wave number for subsequent harmonics can be found by using the previous solution as the initial guess.

The various parts of the calculation can be grouped for speed of execution:

Constant terms and run parameters

$$\text{const term} = \frac{16\pi U}{Wg}$$

$$K_0 = \frac{g}{U^2}$$

Harmonic term

$$\text{harm term} = \frac{K_0 + K_m \cos^2 \theta_m}{1 + \sin^2 \theta_m - K_0 H \operatorname{sech}^2(K_m H)}$$

X terms

$$\text{x term} \xi_m = \cos(K_m x_\sigma \cos \theta_m)$$

$$\text{x term} \eta_m = \sin(K_m x_\sigma \cos \theta_m)$$

Y term

$$\text{y term} \cos \frac{m \pi y_\sigma}{W} \text{ , for even } m$$

$$\text{y term} \sin \frac{m \pi y_\sigma}{W} \text{ , for odd } m$$

noting that the term for $m = 0$ is halved.

Z term

$$\text{z term} = e^{-K_m H} \cosh [K_m (H - h_\sigma)] = \tfrac{1}{2} \left[e^{-K_m h_\sigma} + e^{K_m (h_\sigma - 2H)} \right]$$

where $h_\sigma = -z_\sigma$

APPENDIX C

C Virtual Appendage Transom Stern Model

An alternative approach for closing the transom stern and modelling the separated flow behind the transom was to add a fictitious appendage to the aft end of the model. The virtual appendage enclosed the separated and stagnated flow in the case of the slow speed flow regime, and the air pocket in the high speed range (see Figure 9). The potential flow was then modelled around the new shape.

The horizontal planar flow around the transom was considered by examining the two dimensional flow over a backward facing step (see Figure 10). It was noted by Batchelor[2] and Sinha[7] that the re-attachment length (L_R) tends to six times the step height (h) for high Reynolds number turbulent flow. The transom stern body was closed by the addition of an extra point down stream of the transom for each water line, the down stream offset being six times the transom half breadth (see Figure 11).

Although the initial motivation for the development of this model was to improve the prediction of wave pattern resistance at slow speed, it also proved very effective at high speed. The basic model (with fixed re-attachment length:transom half-breadth ratio of 6) gave good results for for all models in both monohull and catamaran configurations. Predictions for the lower B/T models were better than for the wider models. This was probably due to the two dimensional flow approximation, the models with the more deeply immersed transom being less affected by non xy-plane flow and free surface effects. Examination of the results from the sink-line transom model (where sinks were closely placed on the transom itself) showed over estimates of wave pattern resistance. Thus potential improvements to the model may be achieved by the adjustment of the re-attachment length (as a proportion of the transom beam) as a function of breadth:draught ratio and perhaps also Froude number. Detailed examination of the transom flow during tank tests would provide useful additional information for this technique. Figure 2 shows an example comparison of the various transom correction methods, and the promising results, over much of the speed range for predicting C_{WP} by the virtual appendage method.

Some results of wave pattern resistance predictions using this model are presented in Figures 12 to 14. It can be seen that predictions of wave pattern resistance over the whole speed range are very good. However from a practical designer's point of view, prediction of wave resistance, including the additional resistance at $Fn < 0.4$, would be more useful since only $(1+k)C_F$ would have to be added to obtain the total resistance. Relating the wave pattern resistance to the wave resistance using a regression analysis of the experimental results[6] offers a potential solution. This has been attempted and the initial results look promising.

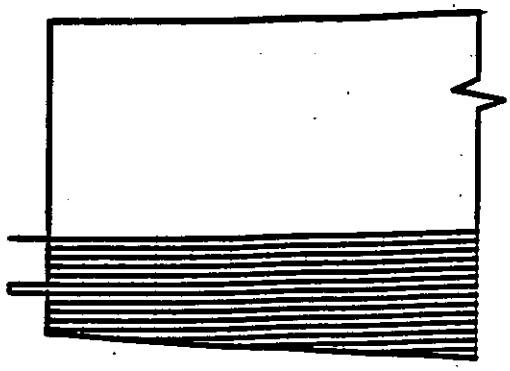

A single sink at half transom draught

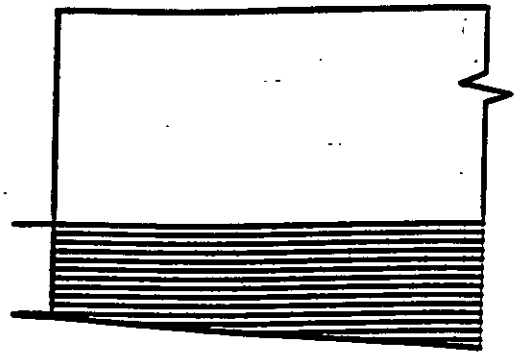

A single sink at full transom draught

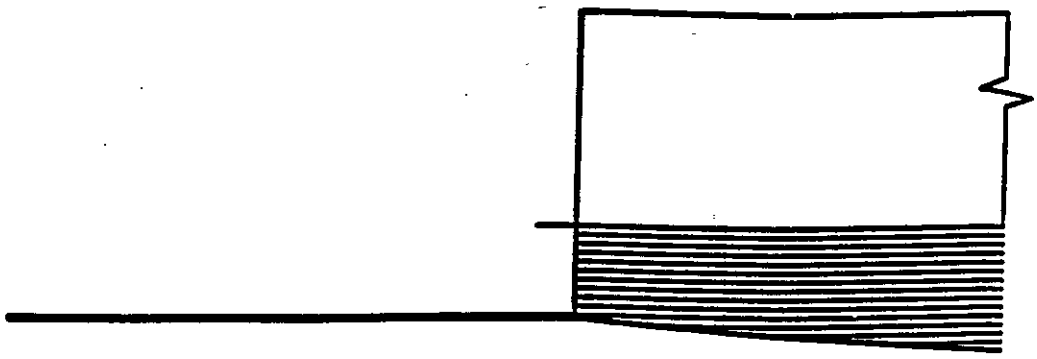

A single trailing line of sinks at full transom draught

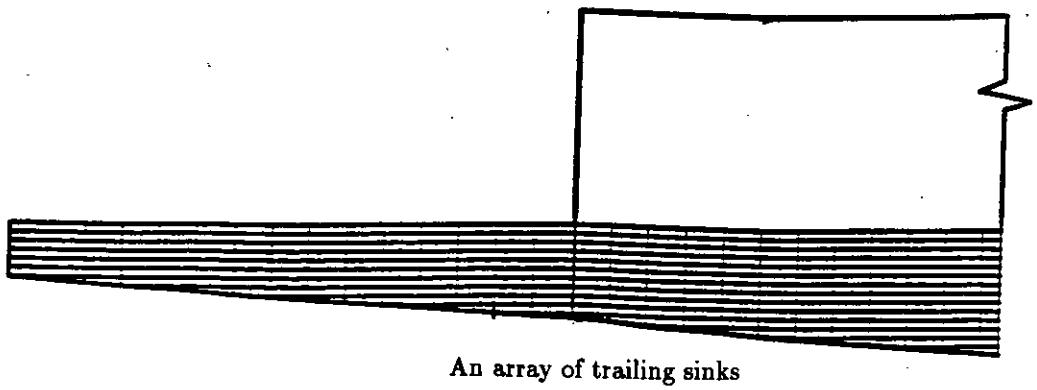

An array of trailing sinks

Figure 1: Examples of sink arrays used to model transom resistance

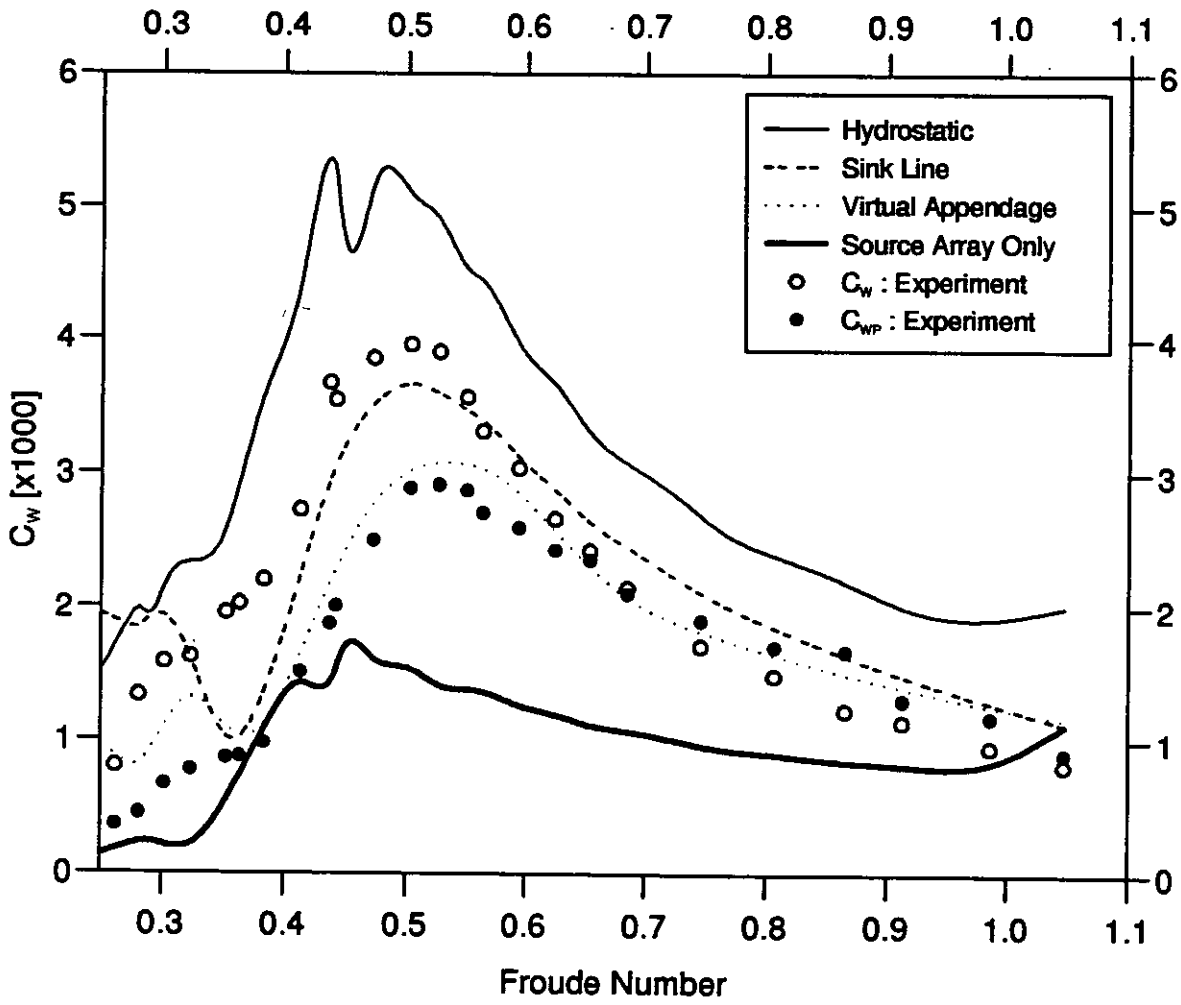

Figure 2: Comparison of the effect on C_W of the different theoretical models used for the transom

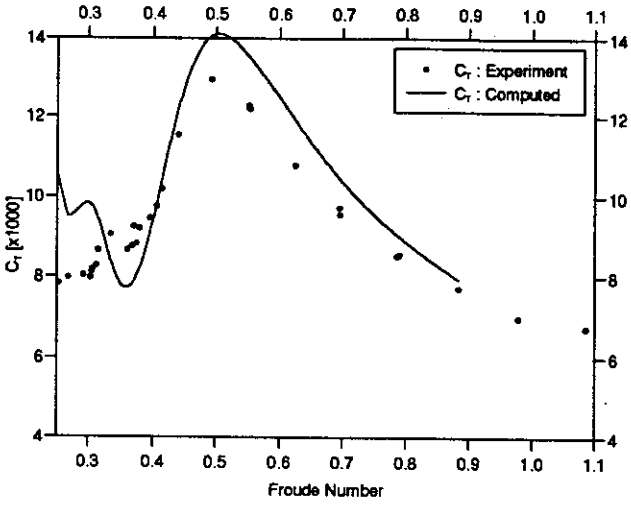

Figure 3a: Model 3b Monohull

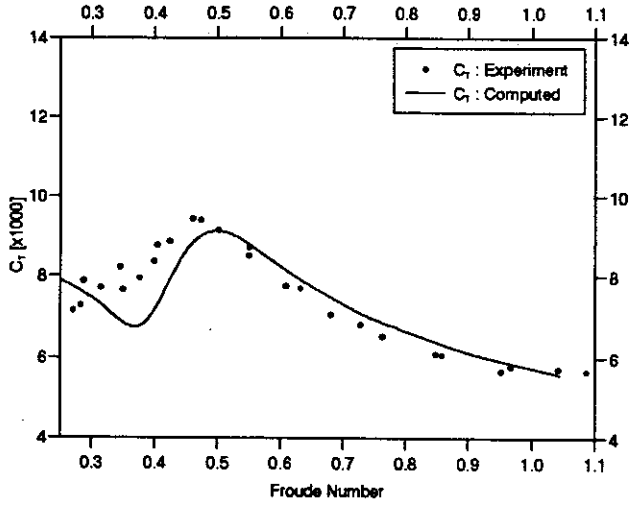

Figure 3b: Model 4b Monohull

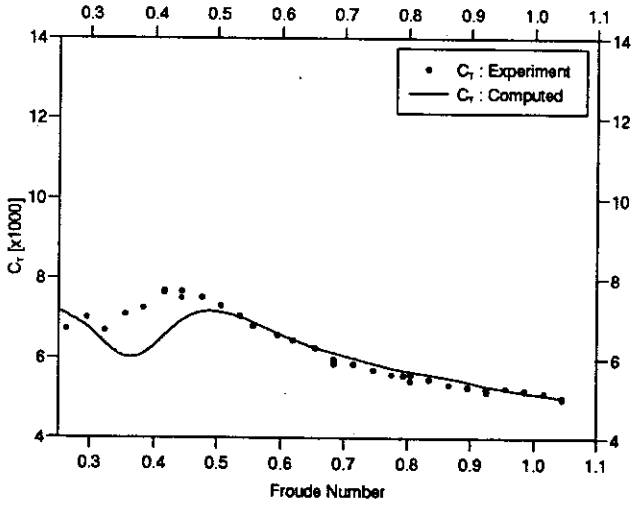

Figure 3c: Model 5b Monohull

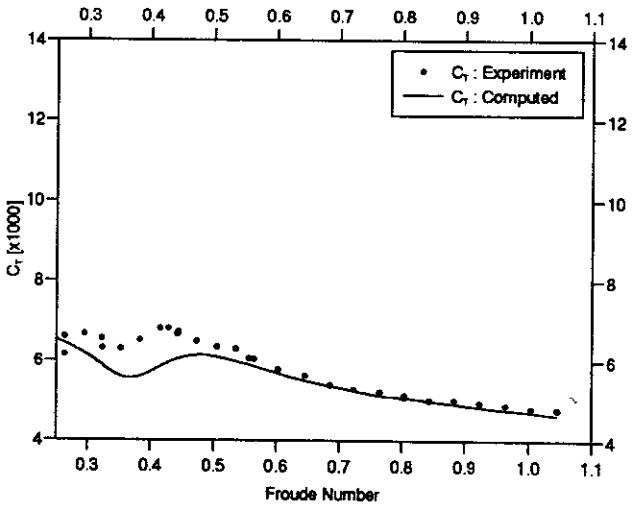

Figure 3d: Model 6b Monohull

Figure 3: Comparison of theoretical predictions of C_T (using the sink line transom correction) with experimental results — Effect of Length:Displacement Ratio (monohulls)

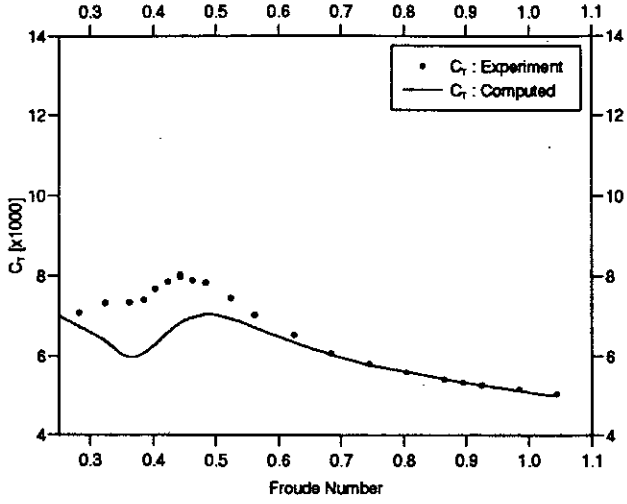

Figure 4a: Model 5a Monohull

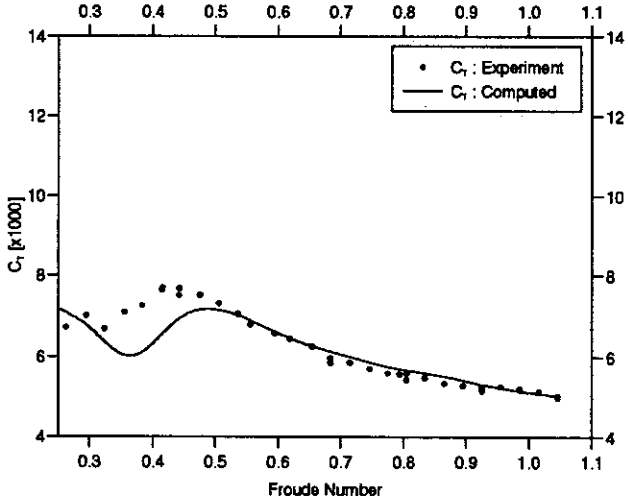

Figure 4b: Model 5b Monohull

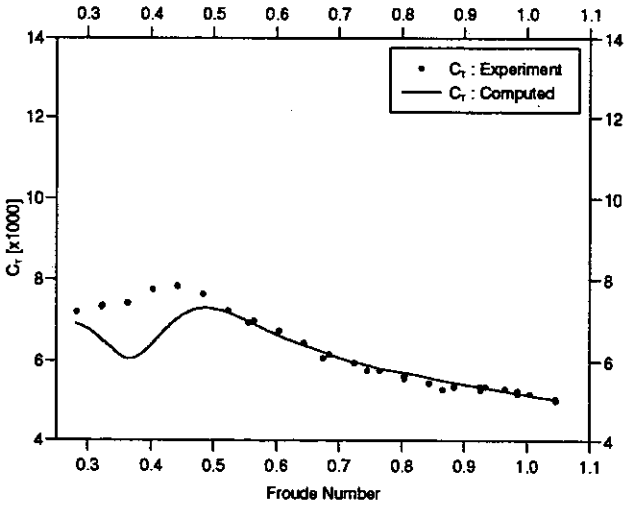

Figure 4c: Model 5c Monohull

Figure 4: Comparison of theoretical predictions of C_T (using the sink line transom correction) with experimental results — Effect of Breadth:Draught Ratio (monohulls)

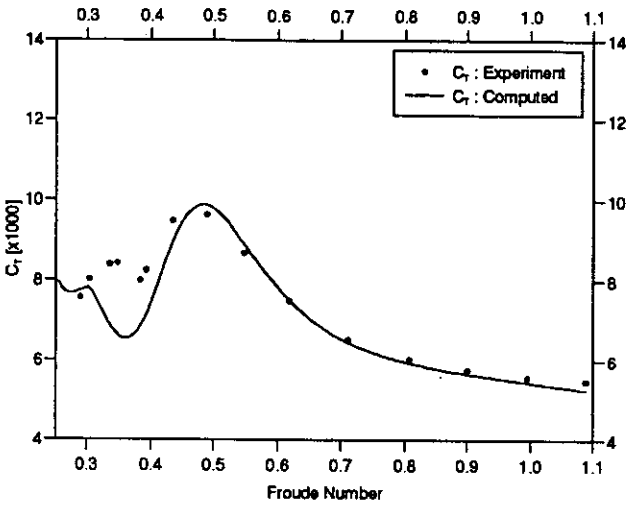

Figure 5a: Model 5b $S/L = 0.2$

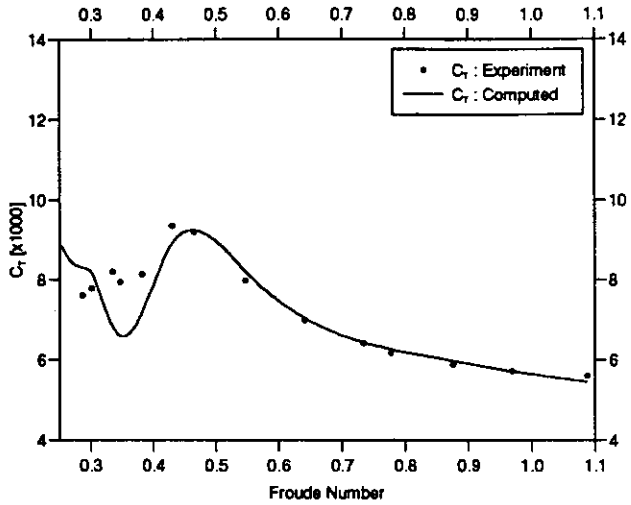

Figure 5b: Model 5b $S/L = 0.3$

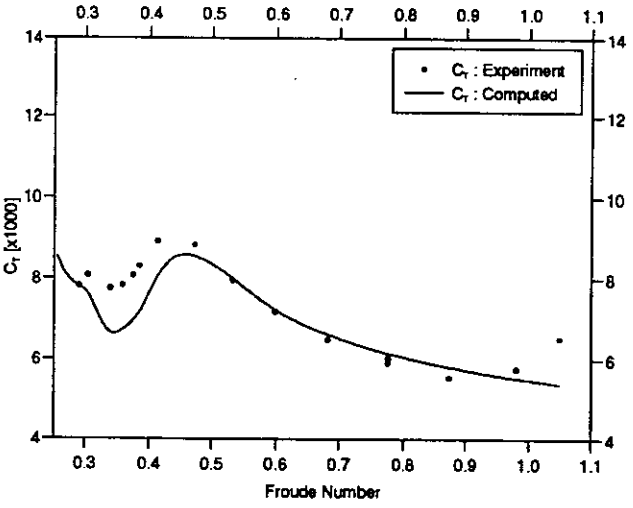

Figure 5c: Model 5b $S/L = 0.4$

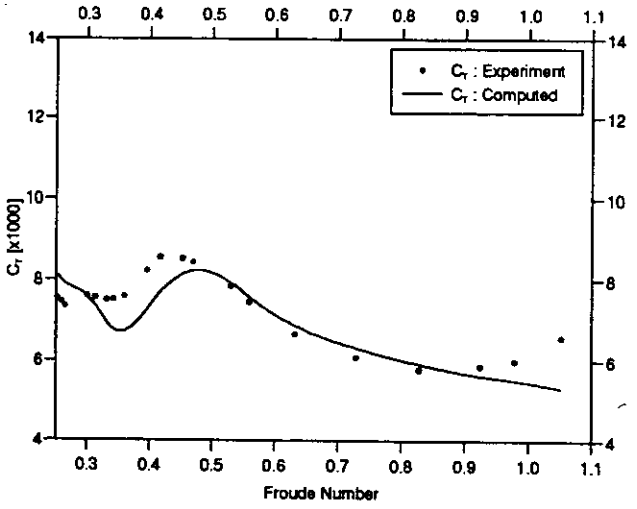

Figure 5d: Model 5b $S/L = 0.5$

Figure 5: Comparison of theoretical predictions of C_T (using the sink line transom correction) with experimental results — Effect of Separation:Length Ratio (catamarans)

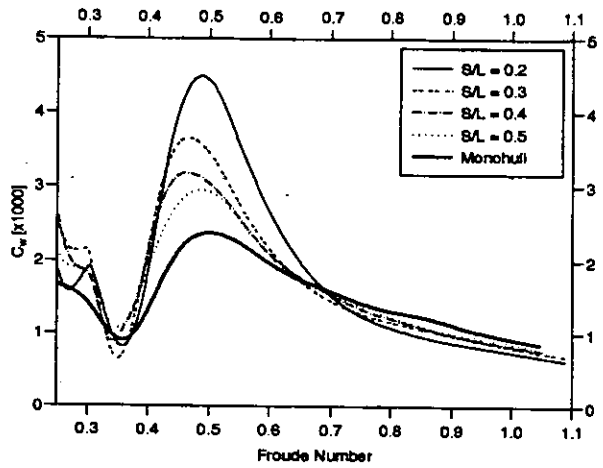

Figure 6a: Models 5b Sink Line Model

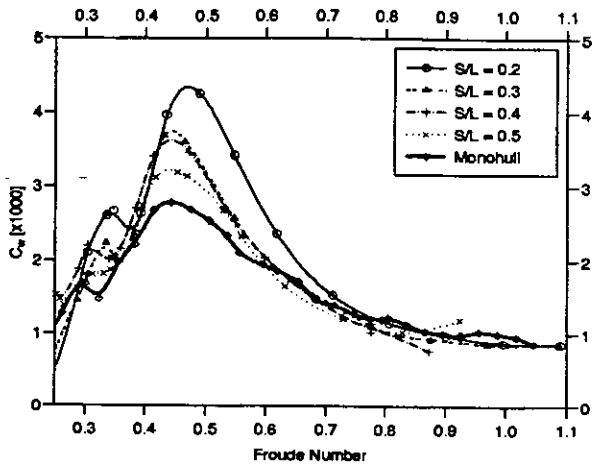

Figure 6b: Models 5b Experiment

Figure 6: Comparison of C_W — Effect of Separation:Length Ratio

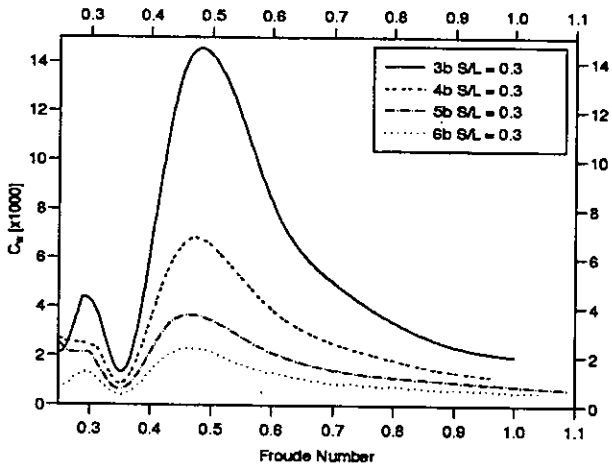

Figure 7a: Models 3,4,5,6b $S/L = 0.3$ Sink Line Model

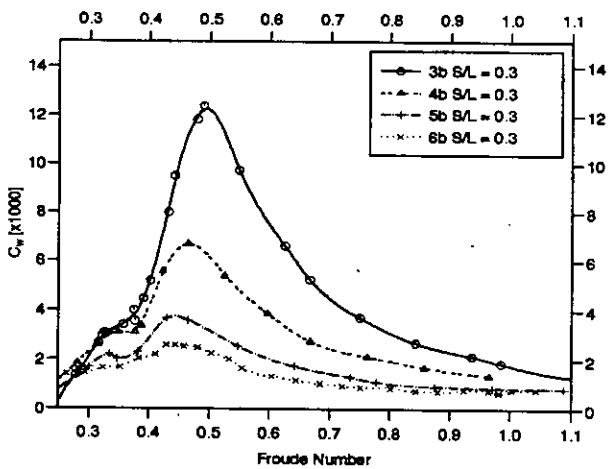

Figure 7b: Models 3,4,5,6b $S/L = 0.3$ Experiment

Figure 7: Comparison of C_W — Effect of Length:Displacement Ratio

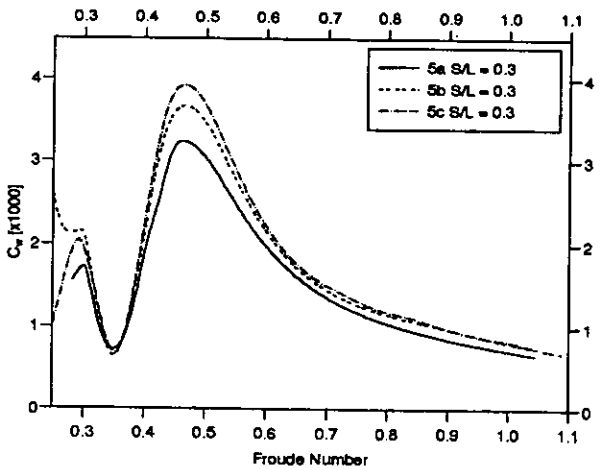

Figure 8a: Models 5a,b,c $S/L = 0.3$ Sink Line Model

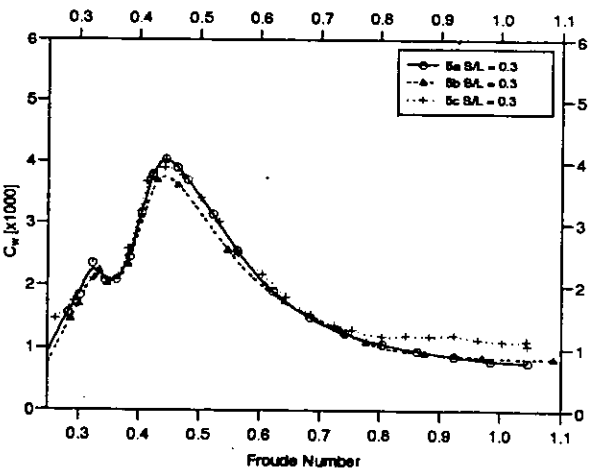

Figure 8b: Models 5a,b,c $S/L = 0.3$ Experiment

Figure 8: Comparison of C_W — Effect of Breadth:Draugh Ratio

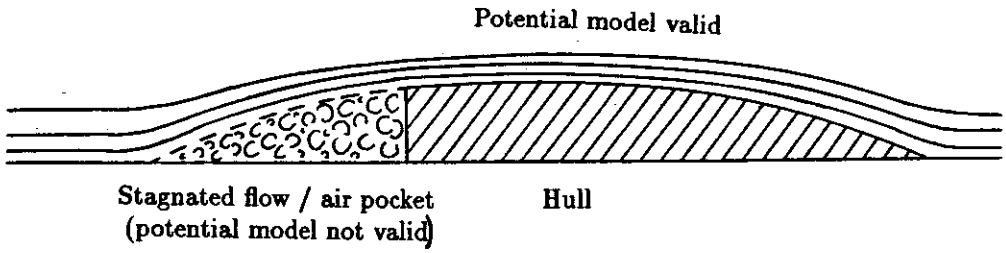

Figure 9: Separated Flow and Air Pocket Behind the Transom

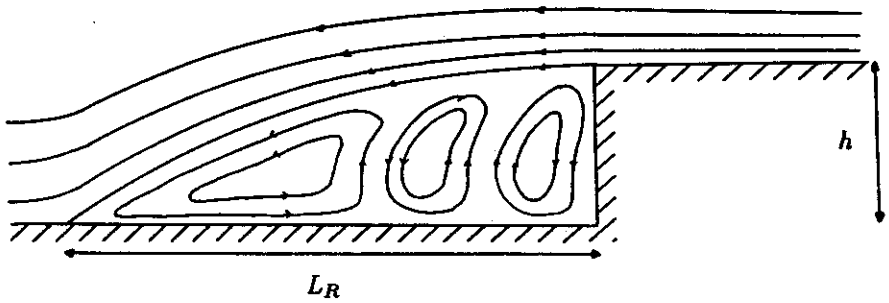

Figure 10: Flow Over a Backward Facing Step

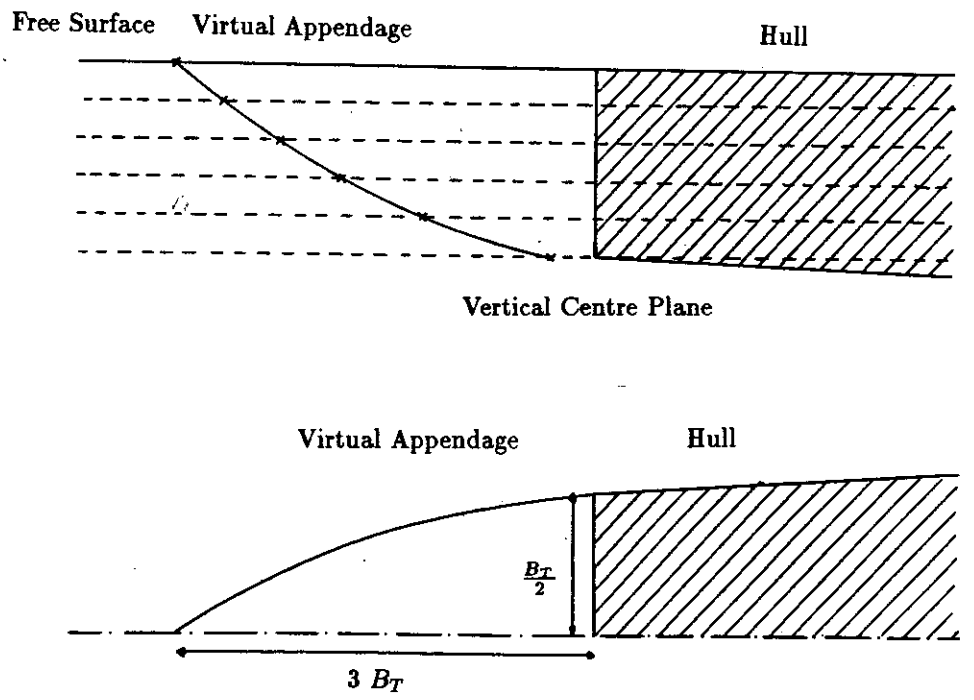

Figure 11: Virtual Appendage Added Down Stream of Transom

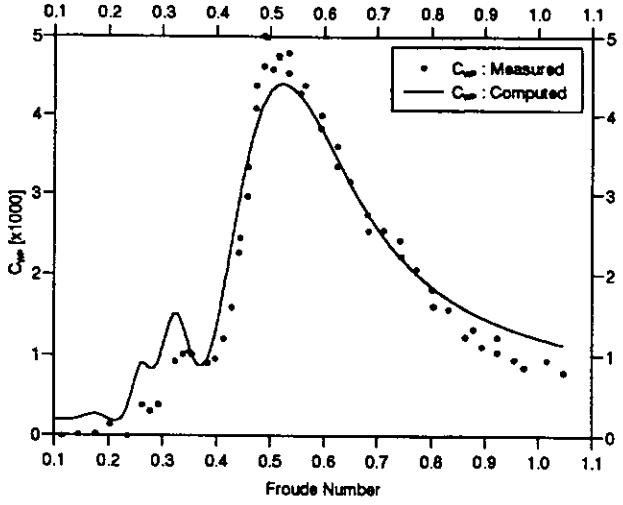

Figure 12a: Models 4a $S/L = 0.2$

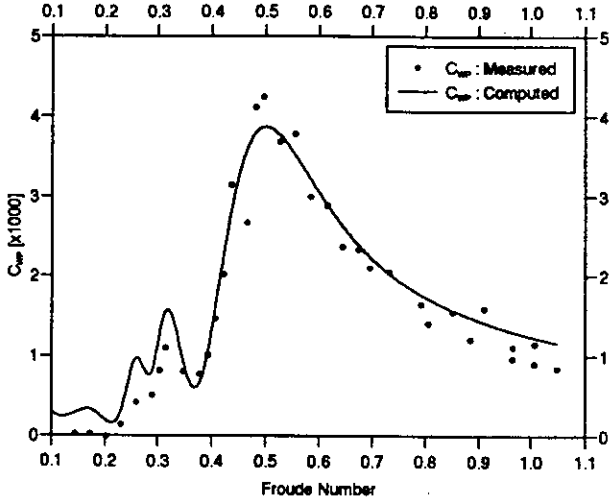

Figure 12b: Models 4a $S/L = 0.3$

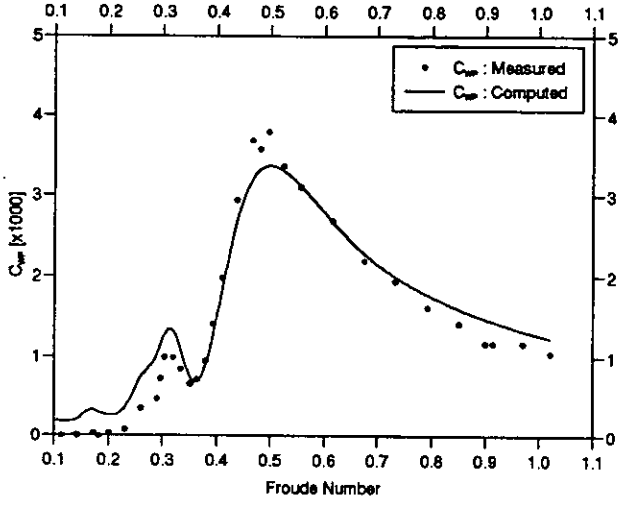

Figure 12c: Models 4a $S/L = 0.4$

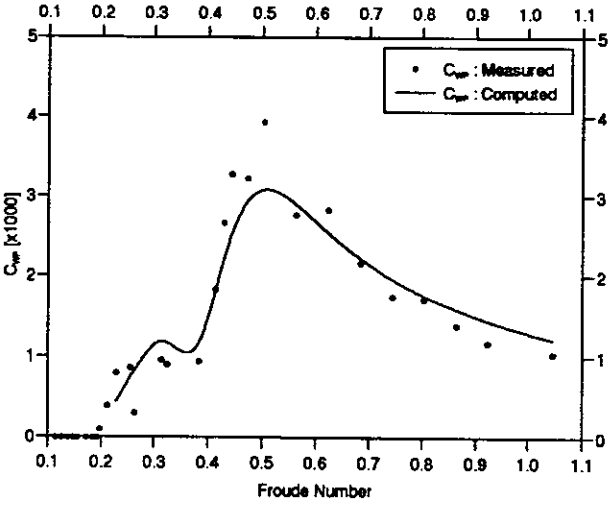

Figure 12d: Models 4a $S/L = 0.5$

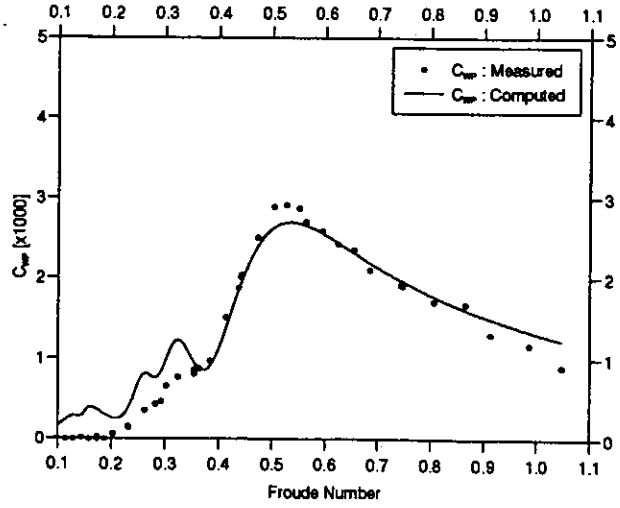

Figure 12e: Model 4a Monohull

Figure 12: Comparison of theoretical predictions of C_{WP} with experimental results
Virtual Appendage Model - Models 4a

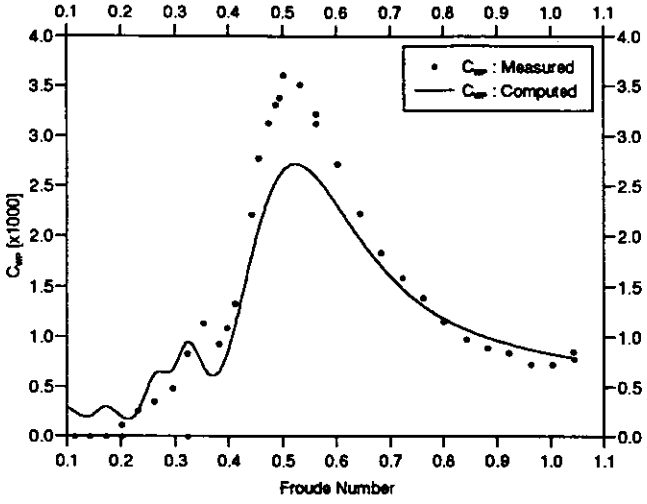

Figure 13a: Models 5c $S/L = 0.2$

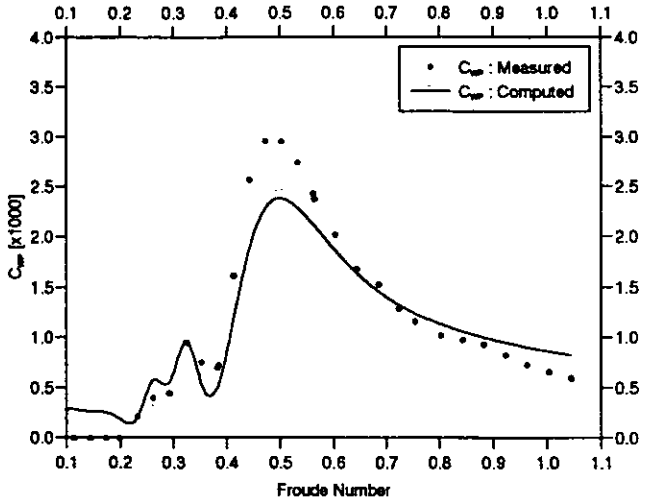

Figure 13b: Models 5c $S/L = 0.3$

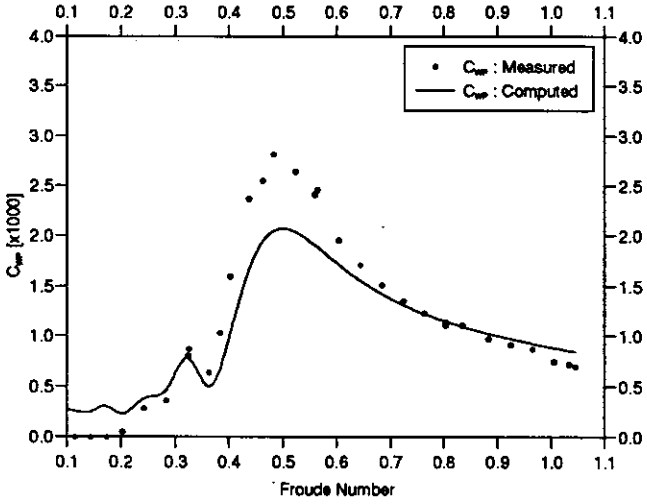

Figure 13c: Models 5c $S/L = 0.4$

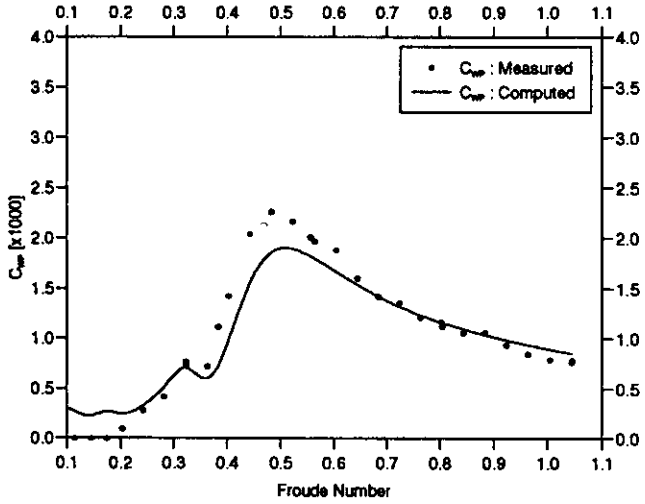

Figure 13d: Models 5c $S/L = 0.5$

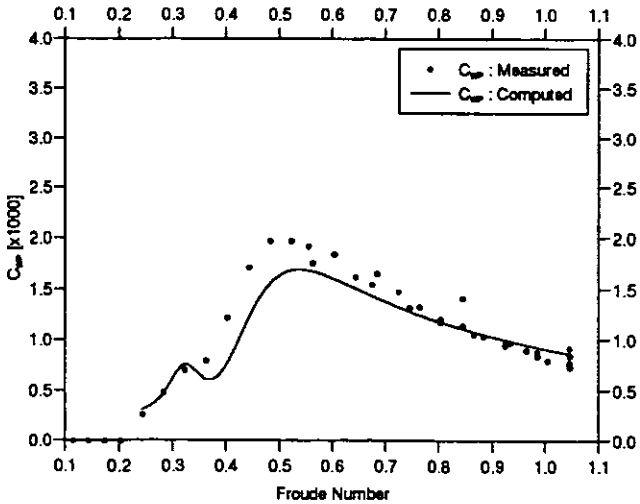

Figure 13e: Model 5c Monohull

Figure 13: Comparison of theoretical predictions of C_{WP} with experimental results
Virtual Appendage Model - Models 5c

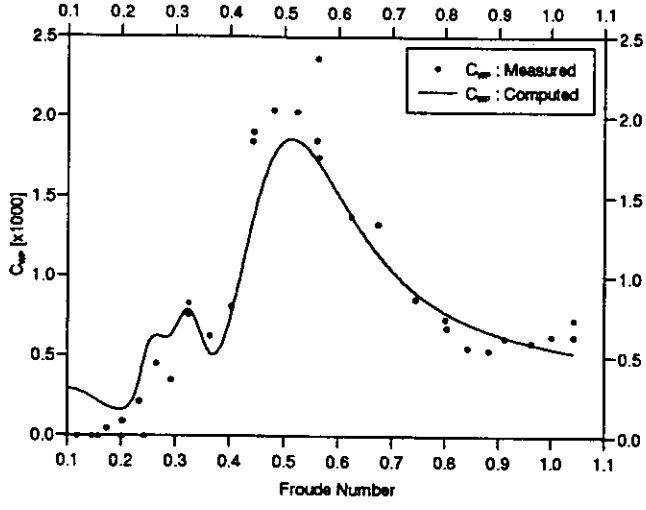

Figure 14a: Models 6b $S/L = 0.2$

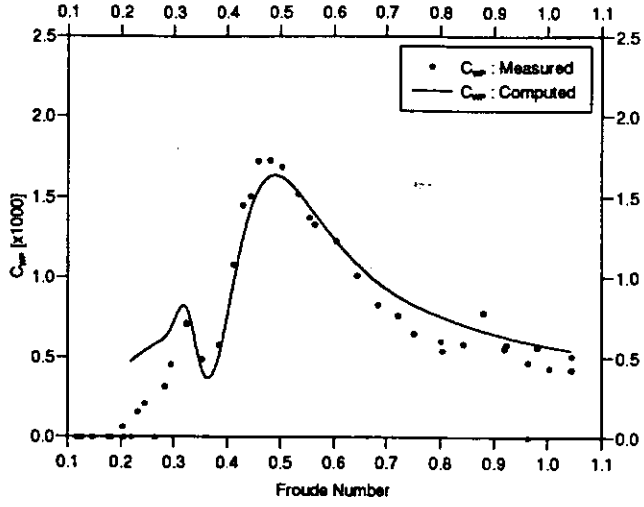

Figure 14b: Models 6b $S/L = 0.3$

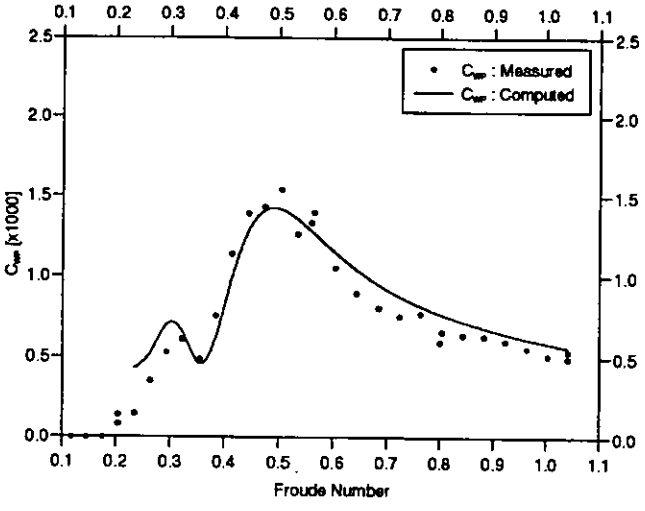

Figure 14c: Models 6b $S/L = 0.4$

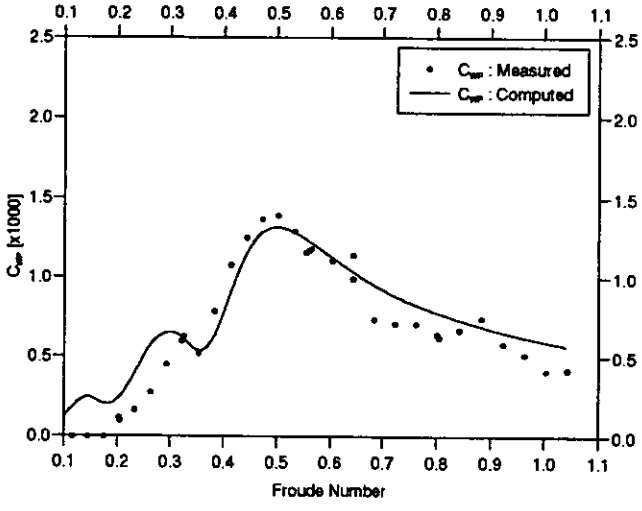

Figure 14d: Models 6b $S/L = 0.5$

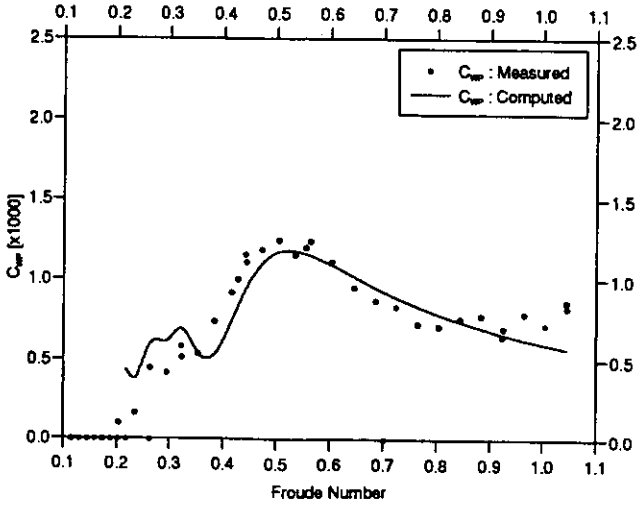

Figure 14e: Model 6b Monohull

Figure 14: Comparison of theoretical predictions of C_{WP} with experimental results
Virtual Appendage Model - Models 6b

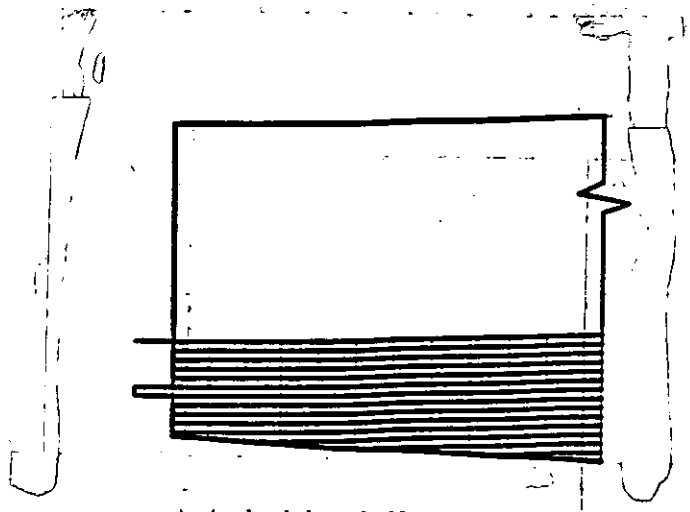

A single sink at half transom draught

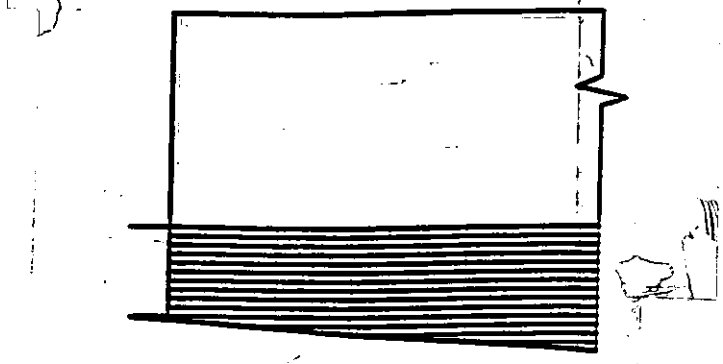

A single sink at full transom draught

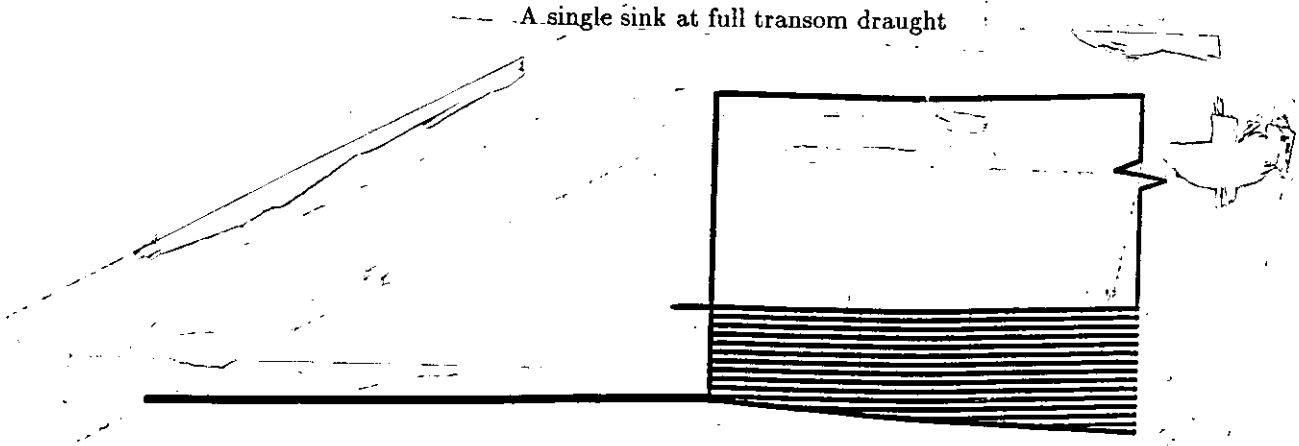

A single trailing line of sinks at full transom draught

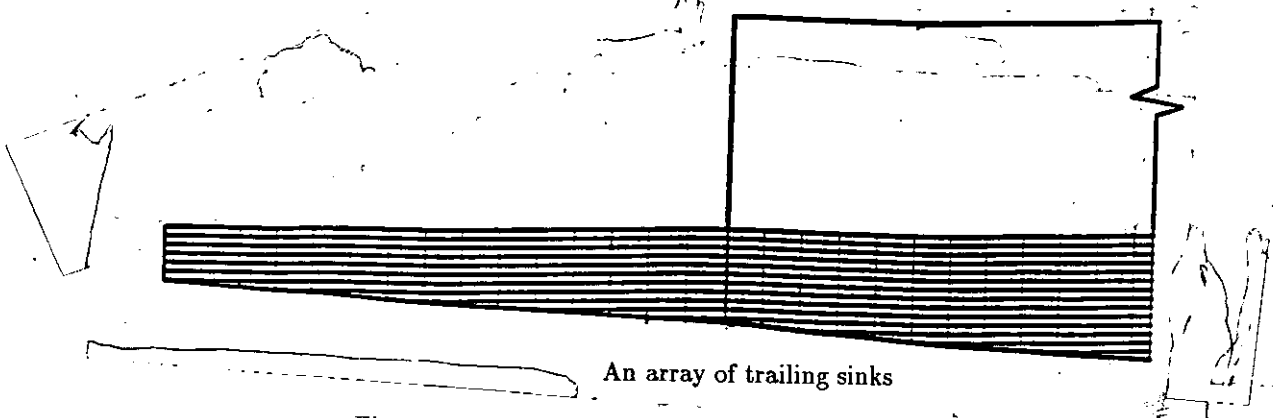

An array of trailing sinks

Figure 1: Examples of sink arrays used to model transom resistance

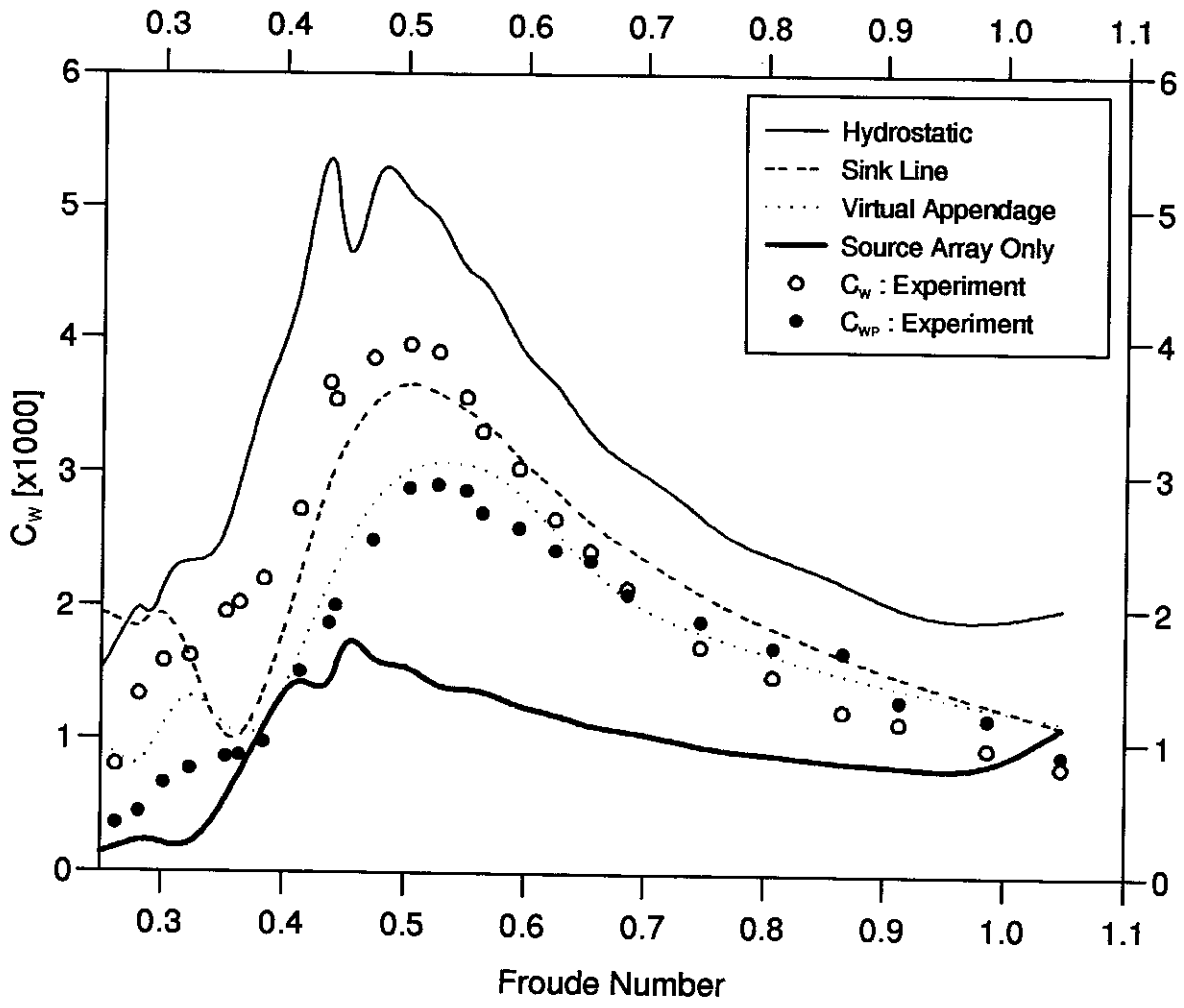

Figure 2: Comparison of the effect on C_W of the different theoretical models used for the transom

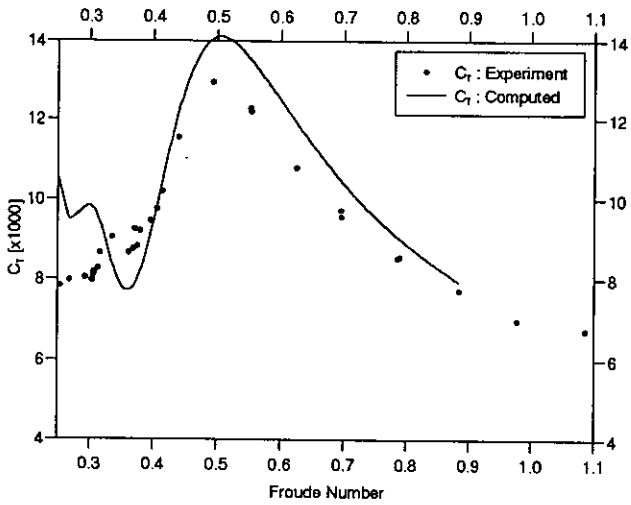

Figure 3a: Model 3b Monohull

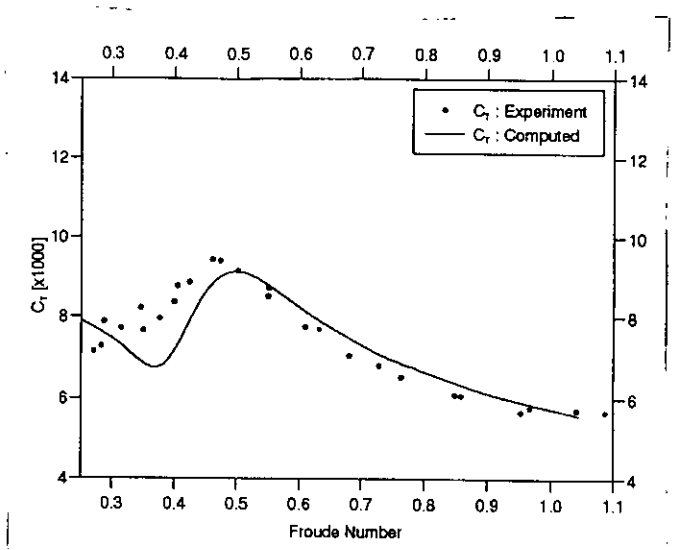

Figure 3b: Model 4b Monohull

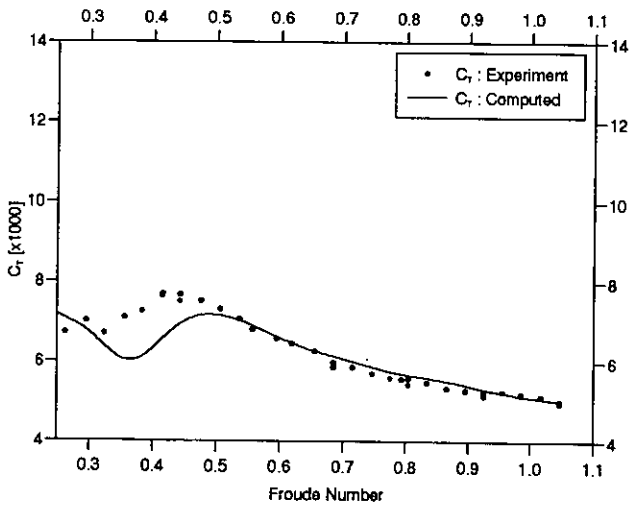

Figure 3c: Model 5b Monohull

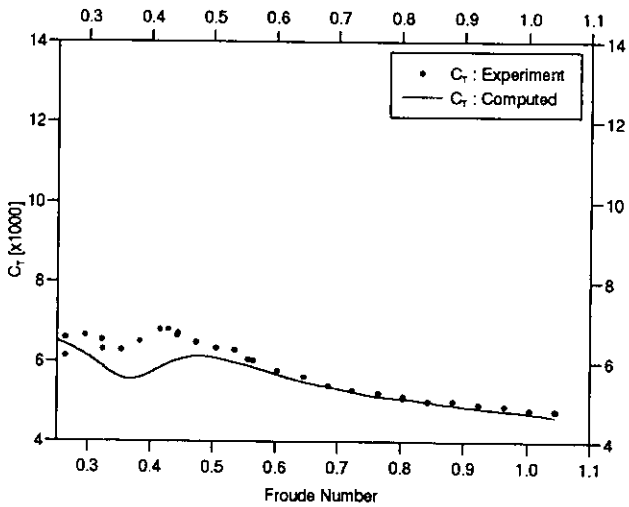

Figure 3d: Model 6b Monohull

Figure 3: Comparison of theoretical predictions of C_T (using the sink line transom correction) with experimental results — Effect of Length:Displacement Ratio (monohulls)

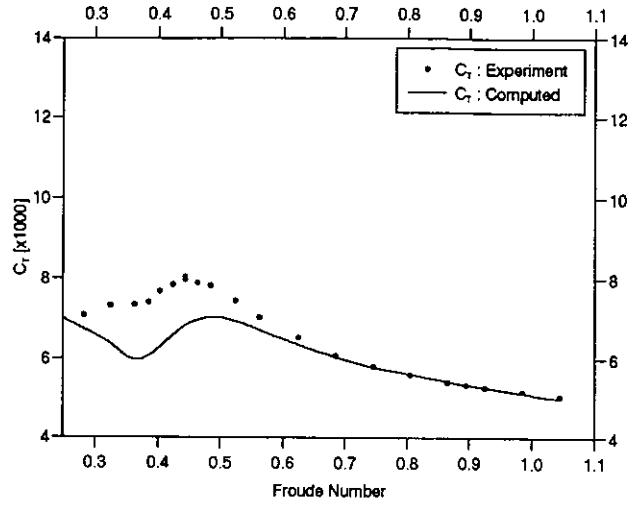

Figure 4a: Model 5a Monohull

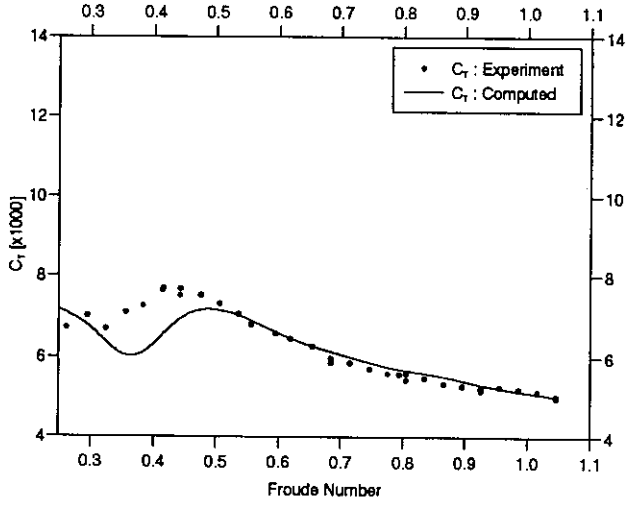

Figure 4b: Model 5b Monohull

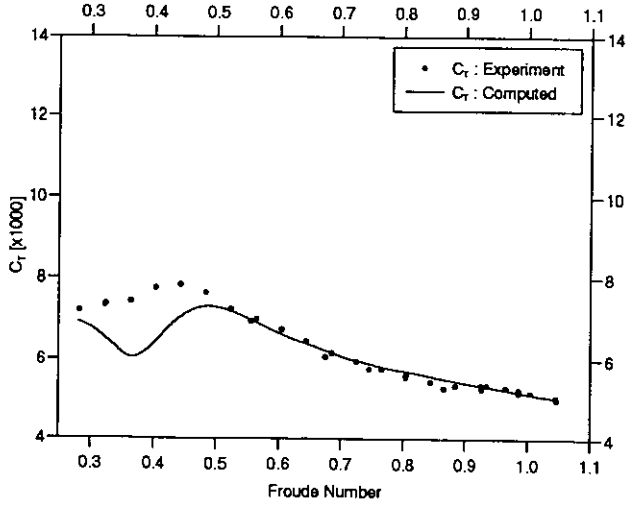

Figure 4c: Model 5c Monohull

Figure 4: Comparison of theoretical predictions of C_T (using the sink line transom correction) with experimental results — Effect of Breadth:Draught Ratio (monohulls)

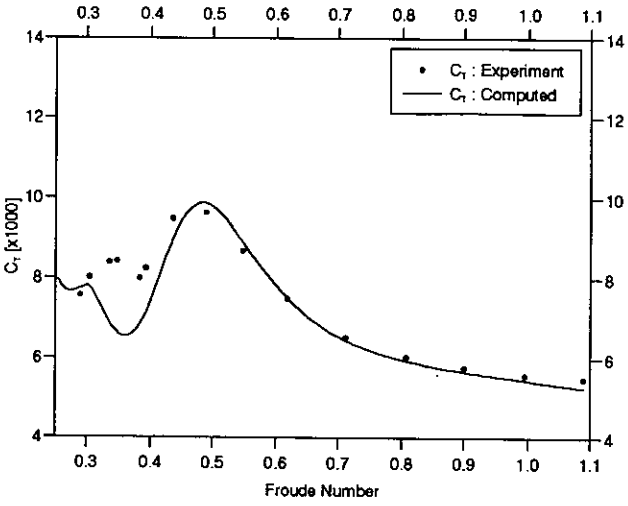

Figure 5a: Model 5b $S/L = 0.2$

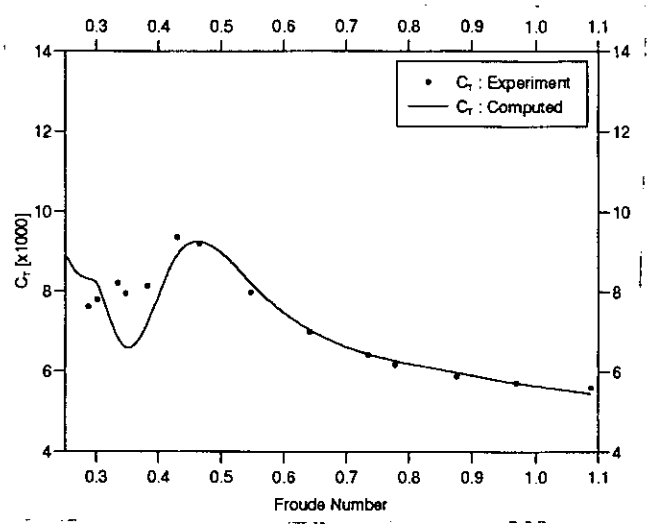

Figure 5b: Model 5b $S/L = 0.3$

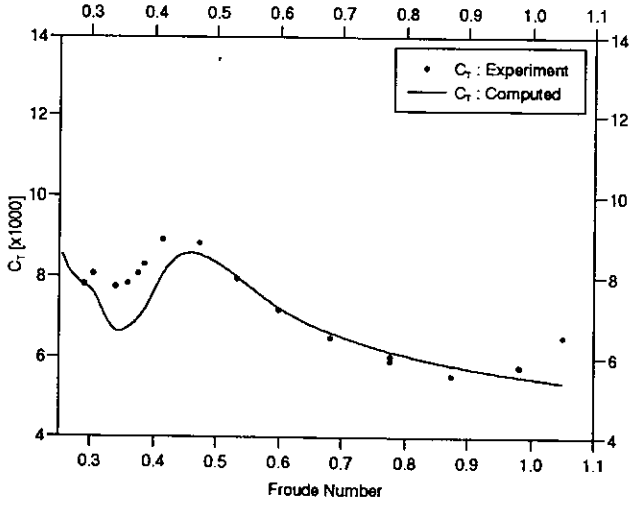

Figure 5c: Model 5b $S/L = 0.4$

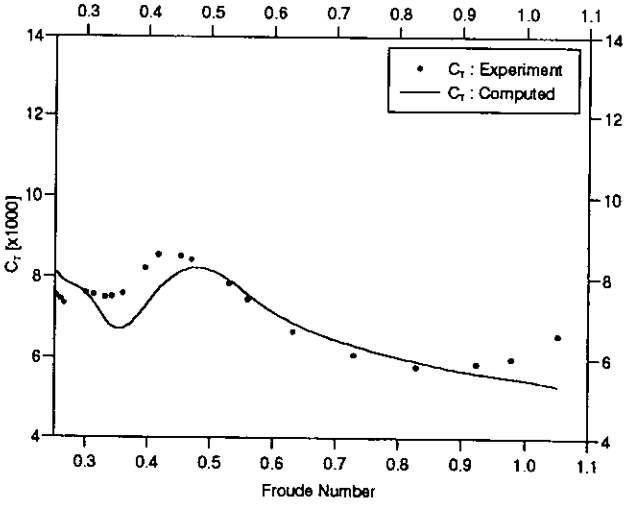

Figure 5d: Model 5b $S/L = 0.5$

Figure 5: Comparison of theoretical predictions of C_T (using the sink line transom correction) with experimental results — Effect of Separation:Length Ratio (catamarans)

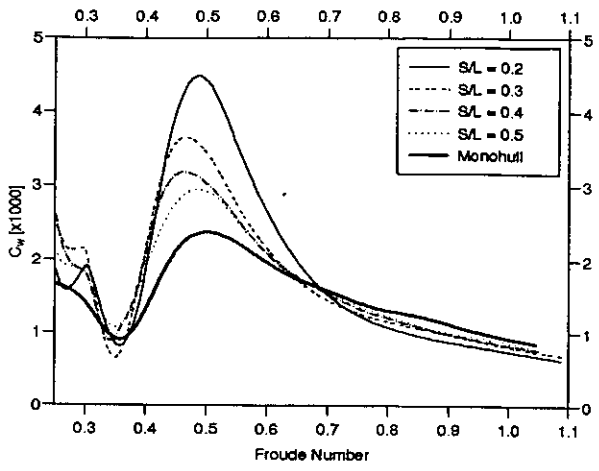

Figure 6a: Models 5b Sink Line Model

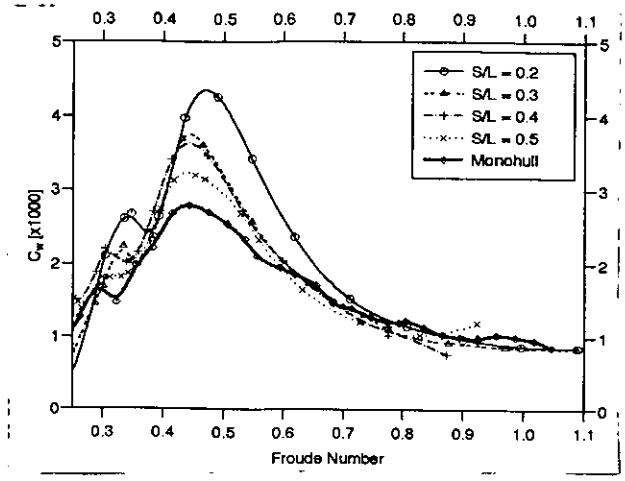

Figure 6b: Models 5b Experiment

Figure 6: Comparison of C_W — Effect of Separation:Length Ratio

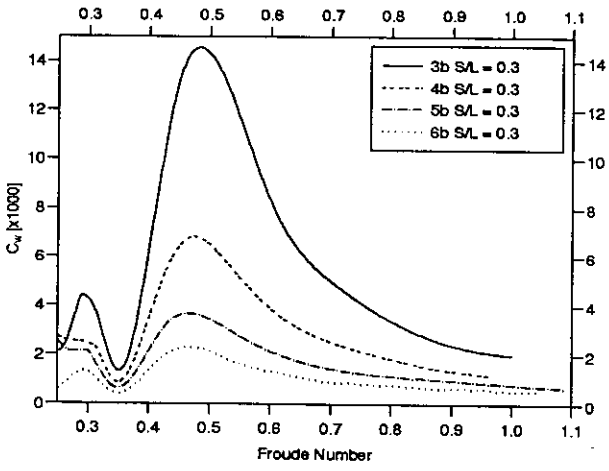

Figure 7a: Models 3,4,5,6b $S/L = 0.3$ Sink Line Model

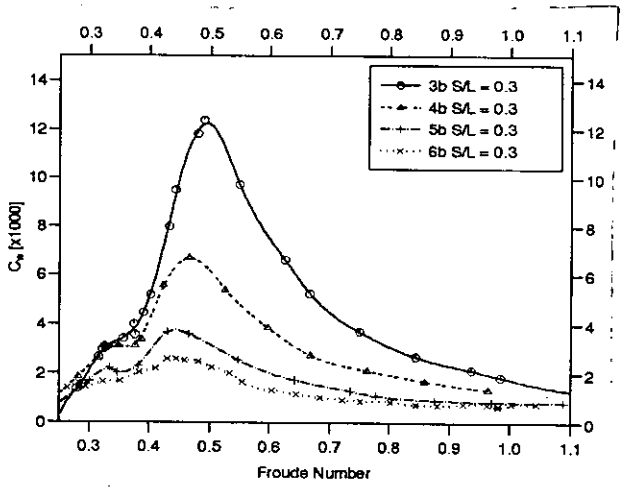

Figure 7b: Models 3,4,5,6b $S/L = 0.3$ Experiment

Figure 7: Comparison of C_W — Effect of Length:Displacement Ratio

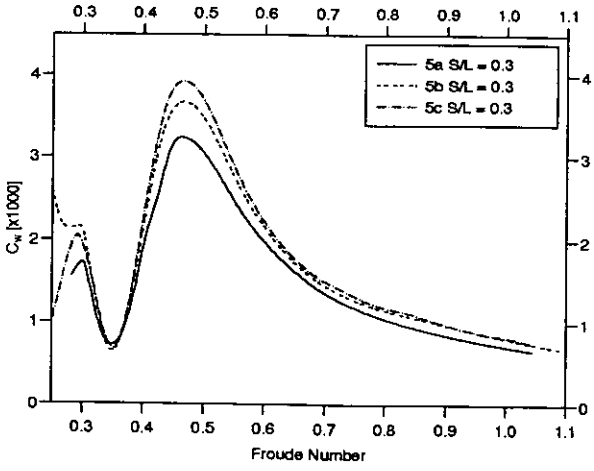

Figure 8a: Models 5a,b,c $S/L = 0.3$ Sink Line Model

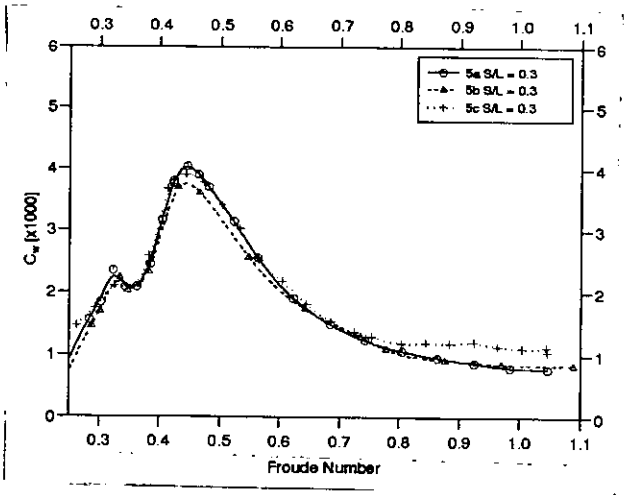

Figure 8b: Models 5a,b,c $S/L = 0.3$ Experiment

Figure 8: Comparison of C_W — Effect of Breadth:Draugh Ratio

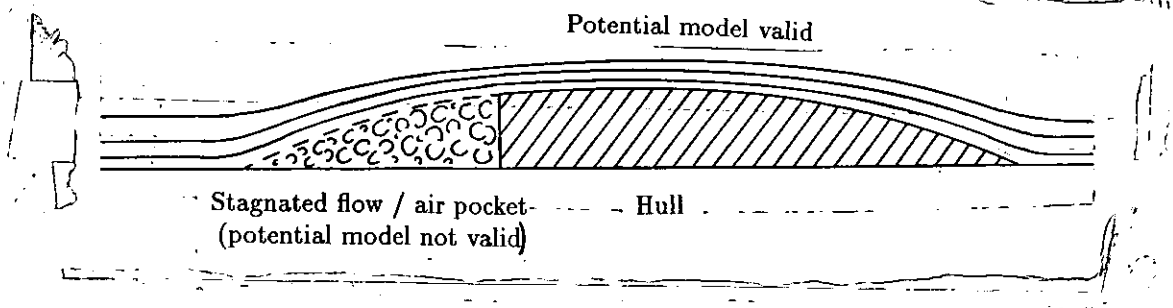

Figure 9: Separated Flow and Air Pocket Behind the Transom

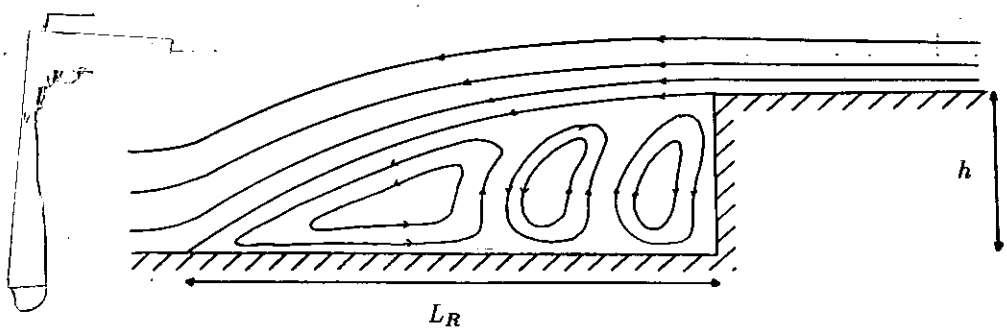

Figure 10: Flow Over a Backward Facing Step

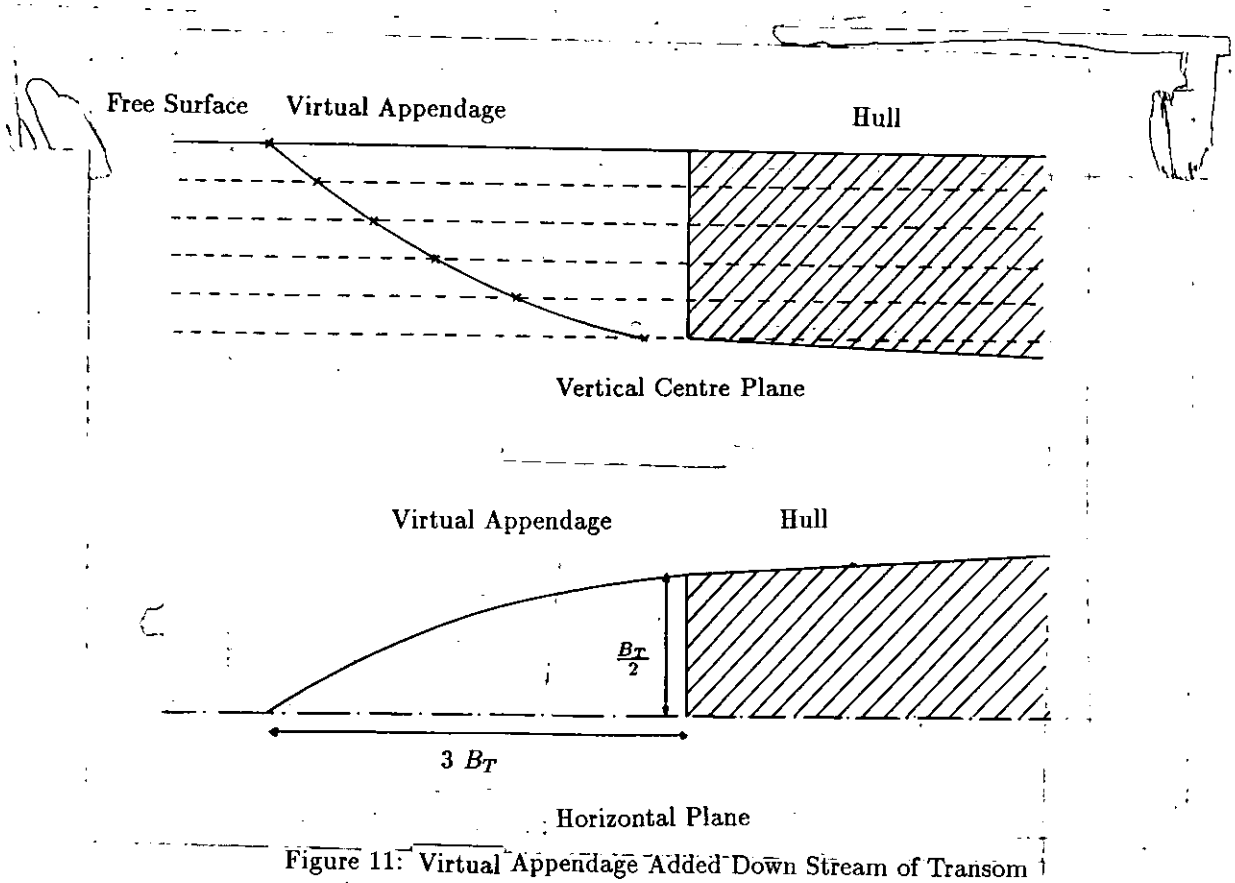

Figure 11: Virtual Appendage Added Down Stream of Transom

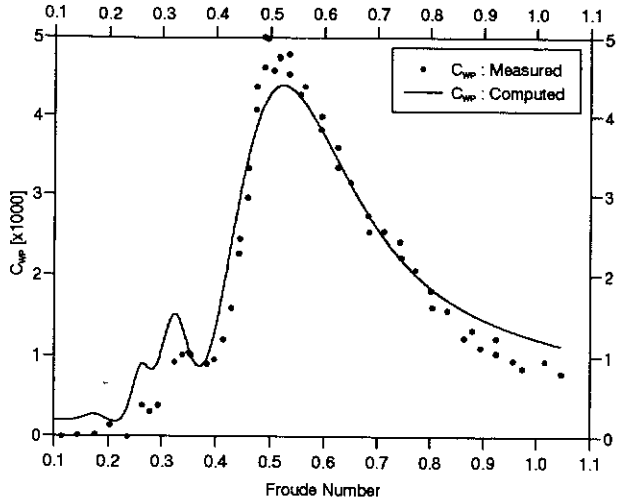

Figure 12a: Models 4a $S/L = 0.2$

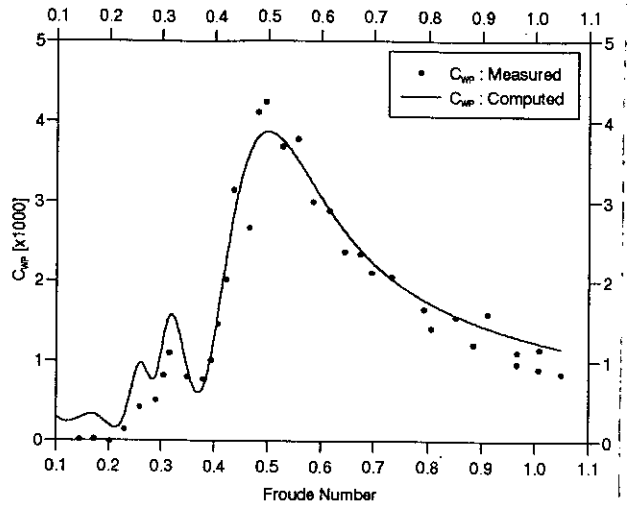

Figure 12b: Models 4a $S/L = 0.3$

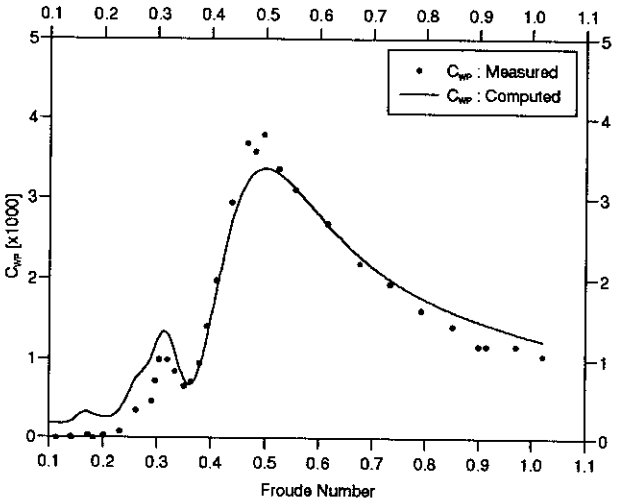

Figure 12c: Models 4a $S/L = 0.4$

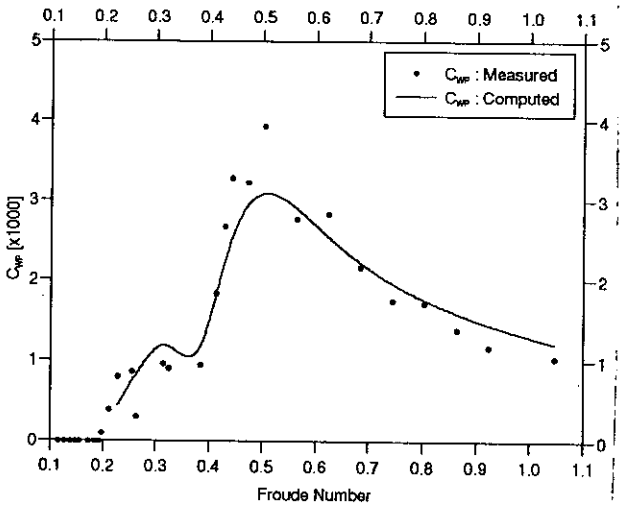

Figure 12d: Models 4a $S/L = 0.5$

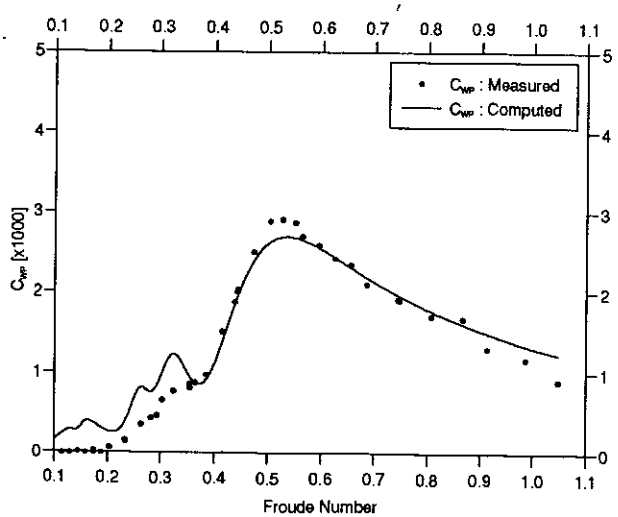

Figure 12e: Model 4a Monohull

Figure 12: Comparison of theoretical predictions of C_{WP} with experimental results
Virtual Appendage Model - Models 4a

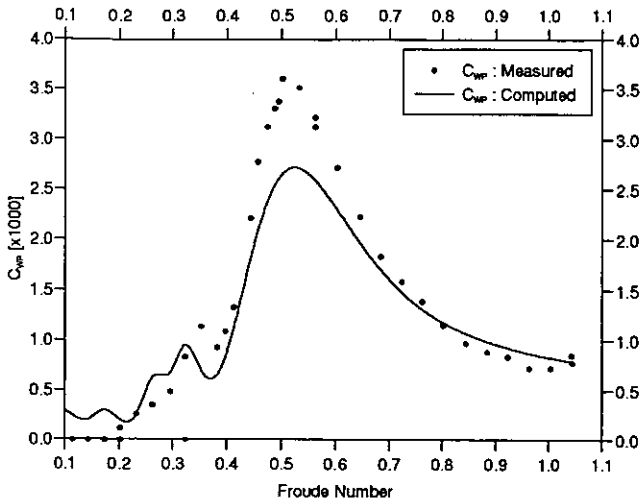

Figure 13a: Models 5c $S/L = 0.2$

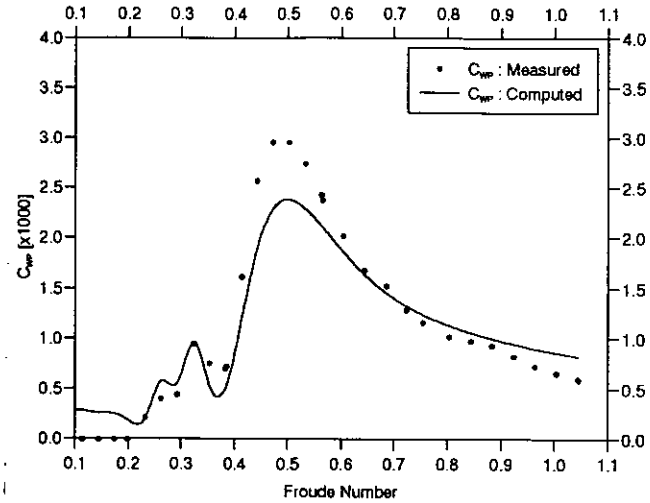

Figure 13b: Models 5c $S/L = 0.3$

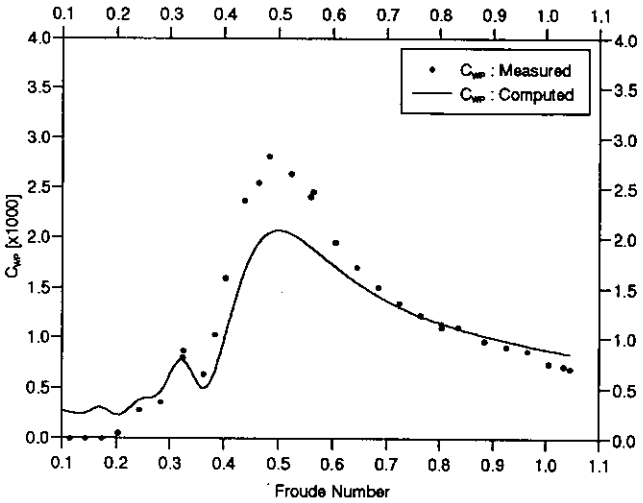

Figure 13c: Models 5c $S/L = 0.4$

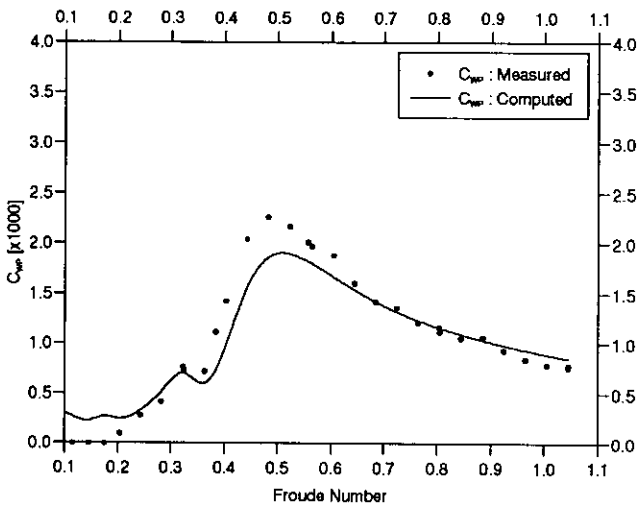

Figure 13d: Models 5c $S/L = 0.5$

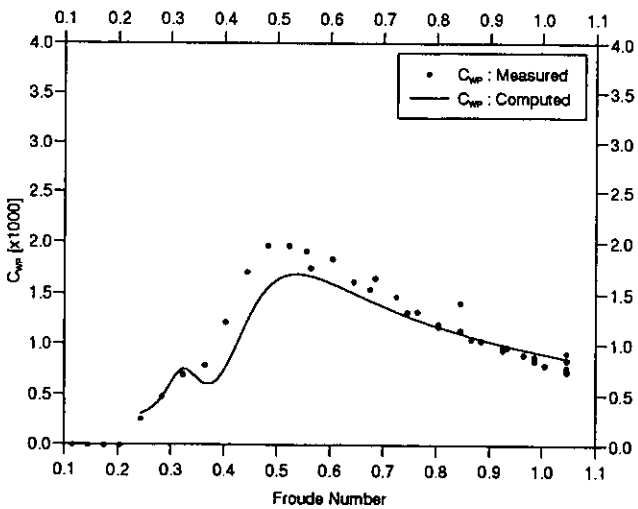

Figure 13e: Model 5c Monohull

Figure 13: Comparison of theoretical predictions of C_{WP} with experimental results
Virtual Appendage Model - Models 5c

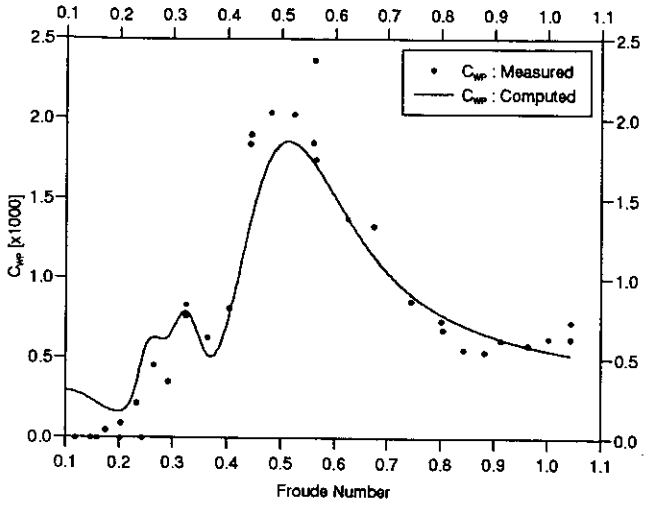

Figure 14a: Models 6b $S/L = 0.2$

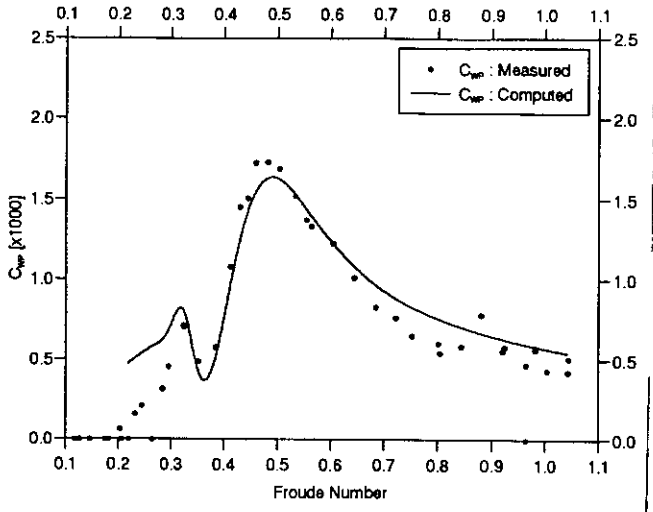

Figure 14b: Models 6b $S/L = 0.3$

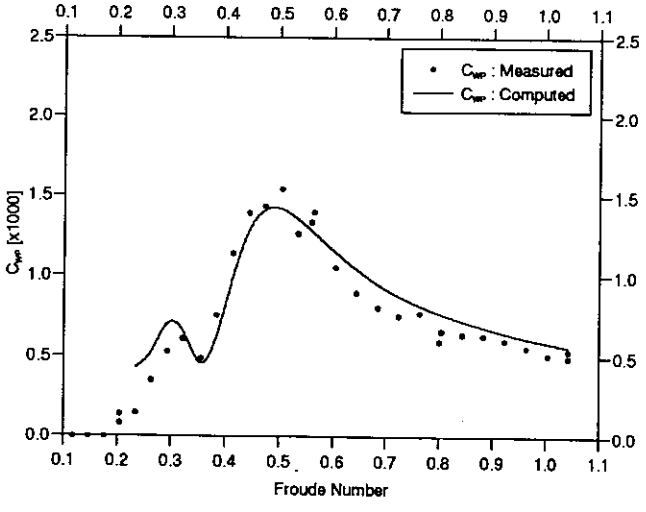

Figure 14c: Models 6b $S/L = 0.4$

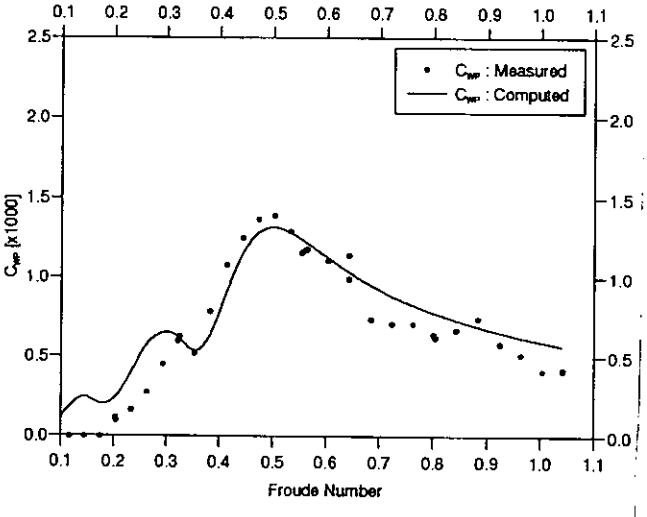

Figure 14d: Models 6b $S/L = 0.5$

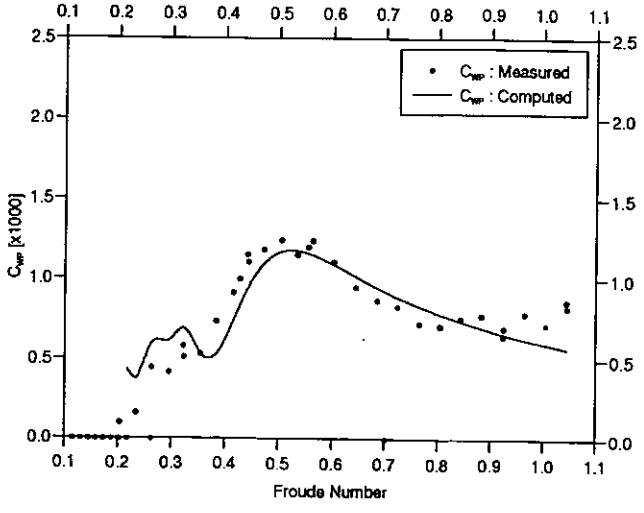

Figure 14e: Model 6b Monohull

Figure 14: Comparison of theoretical predictions of C_{WP} with experimental results
Virtual Appendage Model - Models 6b